METABOLISM

Metabolic adaptation to calorie restriction

Carlos Guijas[1]*†, J. Rafael Montenegro-Burke[1]*, Rigo Cintron-Colon[2]*, Xavier Domingo-Almenara[1], Manuel Sanchez-Alavez[2], Carlos A. Aguirre[2], Kokila Shankar[2], Erica L.-W. Majumder[1], Elizabeth Billings[1], Bruno Conti[2,3]†, Gary Siuzdak[1,4]†

Copyright © 2020 The Authors, some rights reserved; exclusive licensee American Association for the Advancement of Science. No claim to original U.S. Government Works

Calorie restriction (CR) enhances health span (the length of time that an organism remains healthy) and increases longevity across species. In mice, these beneficial effects are partly mediated by the lowering of core body temperature that occurs during CR. Conversely, the favorable effects of CR on health span are mitigated by elevating ambient temperature to thermoneutrality (30°C), a condition in which hypothermia is blunted. In this study, we compared the global metabolic response to CR of mice housed at 22°C (the standard housing temperature) or at 30°C and found that thermoneutrality reverted 39 and 78% of total systemic or hypothalamic metabolic variations caused by CR, respectively. Systemic changes included pathways that control fuel use and energy expenditure during CR. Cognitive computing-assisted analysis of these metabolomics results helped to prioritize potential active metabolites that modulated the hypothermic response to CR. Last, we demonstrated with pharmacological approaches that nitric oxide (NO) produced through the citrulline-NO pathway promotes CR-triggered hypothermia and that leucine enkephalin directly controls core body temperature when exogenously injected into the hypothalamus. Because thermoneutrality counteracts CR-enhanced health span, the multiple metabolites and pathways altered by thermoneutrality may represent targets for mimicking CR-associated effects.

INTRODUCTION

Calorie restriction (CR) is a controlled reduction of calorie intake that increases health span and life span across species (*1*). CR also delays the onset and reduces the incidence of several disorders including cancer and cardiovascular and degenerative diseases (*2*–*4*). Determining the mechanisms by which the beneficial effects of CR occur is fundamental in developing strategies to promote health span including the use of endogenous metabolites to mimic the physiological metabolic responses to CR (CR mimetics), as has been proposed with several drugs (*5*).

An important feature of CR is its ability to reduce core body temperature (T_b). Endotherms maintain a nearly constant T_b by balancing heat production and dissipation. However, during CR, they reduce T_b, a phenomenon observed in humans, nonhuman primates, and rodents (*6*–*10*). This adaptive response is believed to have evolved to reduce energy expenditure when nutrients are scarce, effectively "gaining time" to find food (*11*, *12*). Time is exactly what the organism gains when experimentally subjected to CR, because life span is prolonged. Research on rodents has demonstrated that T_b reduction is not merely a consequence of CR but also contributes to its beneficial impact. Transgenic mice with lowered T_b have increased median life span independent of CR (*13*) and epidemiology provides support for the notion that low T_b is also associated with longevity in humans. The National Institutes of Aging–funded Baltimore Longitudinal Study of Aging found that participants with lower median body temperatures at study entry live substantially longer than those with higher body temperatures (*8*). An independent study analyzing data from more than 18,000 individuals showed that body temperature is lower in subjects in the oldest cohorts (*14*). The analysis of more than 600,000 human temperature measurements spanning over 150 years (1860–2017) demonstrated that average temperature has decreased 0.03°C per birth decade, alongside with an increase in life span during the same time period (*15*). Last, work in *Drosophila melanogaster* and in *Caenorhabditis elegans* has indicated that the effects of temperature on longevity are not simply thermodynamics but are also mediated by specific biochemical and genetic pathways (*16*–*19*).

Temperature homeostasis is maintained at the expense of energy. That energetic cost is inversely correlated with ambient temperature (T_a). Energetic cost is minimal for mice and humans at 30°C, a value at which both species are thermoneutral. Thermoneutrality minimizes heat loss, thereby preventing the hypothermic response observed during CR at lower T_a.

Endotherms, including humans and mice, tend to prefer to spend most of their time in a thermoneutral comfort zone and do so primarily by behavioral thermoregulation. This includes choosing to occupy or generate T_a that is thermoneutral or near thermoneutrality. Humans achieve this most often with clothing or by regulating T_a. Mice most typically burrow and/or cuddle. Yet, most of our knowledge on the effects of CR comes from experiments carried out in rodents that are single caged and forcibly housed at 22°C and may provide limited information on the mechanisms that regulate health span during CR. Moreover, housing mice at ~30°C suffices to increase inflammation, atherosclerosis, and fatty liver disease during normal feeding (*20*–*22*) and antagonizes the beneficial effects of CR on lymphoma and longevity (*23*).

In this study, we present experiments designed to determine the effects of thermoneutrality on the metabolome during CR. Mice were housed at standard room temperature or at thermoneutrality and were either fed ad libitum (AL) or subjected to CR. Comprehensive untargeted metabolomics was performed on the hypothalamus and on plasma. The hypothalamus was chosen because this brain region

[1]Scripps Center for Metabolomics, The Scripps Research Institute, 10550 North Torrey Pines Road, La Jolla, CA 92037, USA. [2]Department of Molecular Medicine, The Scripps Research Institute, 10550 North Torrey Pines Road, La Jolla, CA 92037, USA. [3]Department of Neuroscience and Dorris Neuroscience Center, The Scripps Research Institute, 10550 North Torrey Pines Road, La Jolla, CA 92037, USA. [4]Departments of Chemistry, Molecular, and Computational Biology, The Scripps Research Institute, 10550 North Torrey Pines Road, La Jolla, CA 92037, USA.
*These authors contributed equally to this work.
†Corresponding author. Email: siuzdak@scripps.edu (G.S.); bconti@scripps.edu (B.C.); carlos.guijas@gmail.com (C.G.)

Downloaded from http://stke.sciencemag.org/ on October 29, 2020

regulates feeding and T_b. We anticipated that some of the changes observed may provide information on pathways that integrate nutrient and temperature homeostasis. Plasma was chosen because it is the effector of the metabolic responses to CR that occur in peripheral tissues, as well as a good indicator of microbiome variability, and thus represents a good vehicle to evaluate system-wide changes. Our hope was that the metabolites identified would include some that could highlight the pathways that may contribute to the antagonizing effects of thermoneutrality on CR. Of the omics disciplines, metabolomics most closely reflects the phenotypic changes, and in addition to its pivotal role in the discovery of altered biochemical pathways, metabolomics has the unique ability of characterizing metabolites that can alter an organism's phenotype (*24*, *25*). We also used artificial intelligence for the post-analysis of metabolomics results, which has been effective for the prediction of metabolites with biological activity (*26*, *27*).

We found that thermoneutrality greatly affected the metabolic changes associated with CR, counteracting nearly 40% of changes in the plasma and up to 78% of changes in the hypothalamus. Many of these metabolites affected by thermoneutrality play a pivotal role in energy exchange with the environment, as well as in fuel consumption and energy expenditure during CR. Moreover, the citrulline–nitric oxide (NO) cycle and leucine enkephalin (LeuEnk) affected T_b.

RESULTS

Overview of untargeted metabolomics results

Untargeted metabolomics analyses were performed on plasma and hypothalamic samples of mice fed AL and CR to 50% of their AL intake, housed at both 22° and 30°C (Fig. 1A). CR was performed by first feeding animals with 100% of the AL diet for 2 days to habituate them to daily rations of food, which was followed by 75% of AL calorie intake for 4 days, and then 50% of AL amounts for the final 8 days before harvesting. During the CR regimen used here, similar body weight reductions were observed in animals housed at 22° and at 30°C (fig. S1A and data file S11), and the ratios between fat or lean body mass and body weight at both temperatures were similar (fig. S1B). At the time of analysis, the body composition was similar between CR animals housed at 22° and 30°C (fig. S1B). Tissues were harvested at three different time points. The onset time point (O, ZT15 to ZT18; ZT, Zeitgeber time) begins a few hours after feeding (ZT12) and is defined by the initiation of T_b reduction for animals housed at 22°C. The maintenance time point (M, ZT23.5 to ZT2.5) is when maximum hypothermia is achieved for mice at 22°C. The termination time point (T, ZT8 to ZT11) is when T_b returns to levels above 34.0°C without feeding or energy input (Fig. 1A, fig. S1C, and data file S7). The same collection time windows were used for the animals housed at 30°C, which showed only a modest T_b change and did not enter into the hypothermia range (T_b < 34.0°C) (Fig. 1A and fig. S1C). Metabolic changes during the three collection points of CR were normalized to the levels of the same metabolites in mice fed AL for each temperature.

More than 20,000 metabolic features were detected by untargeted metabolomics in plasma and the hypothalamus using reversed-phase (RP) and hydrophilic interaction liquid chromatography (HILIC) complementary analytical approaches. Total detected features were subjected to statistical filtering to reveal metabolic features that could represent statistically altered metabolites during CR [q < 0.05, one-way analysis of variance (ANOVA) followed by a local false discovery rate (FDR) correction]. Mice housed at room temperature (22°C) had more statistically significant features than mice housed at thermoneutrality (30°C) (Fig. 1B). Twenty percent of the total features in the hypothalamus of mice housed at 22°C were statistically significant (q < 0.05), compared to only 8.5% of total features at 30°C. Changes with q < 0.01 were 6.5% of the total features in the hypothalamus of mice housed at room temperature and 0.8% in mice housed at thermoneutrality. Similar effects were seen in plasma with 26% of statistically significant (q < 0.05) changes accounted seen at 22°C and 13% seen at 30°C. Changes with a q < 0.01 were 12% at 22°C and 7% at 30°C. Thus, many of the changes in metabolic features due to CR at room temperature were not observed in mice housed at thermoneutrality (Fig. 1B).

After computational annotation of altered features (*28*, *29*) and fragmentation, 90 metabolites were identified from plasma samples and 43 originating from the hypothalamus (Fig. 1C). Among those characterized metabolites, most corresponded to lipids (~40% of total) followed by amino acids, amino acid derivatives, and metabolites engaged in energy metabolism (acylcarnitines and redox cofactors) (Fig. 1C). Even though the total number of metabolites found in plasma was double than that found in the hypothalamus, the relative distribution of metabolite classes remained similar within each tissue (Fig. 1D).

The variation of the metabolites over the three phases of the CR time course (onset, maintenance, and termination) was calculated as the logarithmic fold change of the average peak areas of all metabolites normalized to AL conditions within each housing temperature (data files S1 and S2). Overall, most of the metabolites were decreased during CR at 22°C, and this trend was partially or fully reversed for several metabolites when mice were housed at thermoneutrality, especially in the hypothalamus, as was anticipated by the analysis of altered features (Fig. 1E). Fewer metabolites had increased intensities relative to AL during CR, with the exception of several fatty acids and acylcarnitines in the plasma and two peptides in the hypothalamus (Fig. 1E).

In summary, CR promoted remodeling of the metabolome. These changes were affected by thermoneutrality, providing a framework for the discovery and validation of metabolites that may mediate the hypothermic response to CR or the effects of CR on health span and life span.

Metabolic changes to CR in animals housed at 22°C or at 30°C

Thermoneutral housing is detrimental in several models of disease (*20*–*22*) and antagonizes some of the beneficial effects ascribed to CR (*23*). To make progress toward identifying the changes that may mediate these effects, we compared and subtracted the metabolite changes caused by CR in mice housed at 30°C from those of mice housed at 22°C to find the metabolites whose changes promoted by CR are reverted by thermoneutrality. Metabolites were computationally sorted in three different groups based on the trend of the fold change over time (fig. S2A). Because thermoneutrality prevented the hypothermic response, those metabolites that were altered at 30°C but not at 22°C or vice versa were arbitrarily classified as temperature dependent. In contrast, metabolites that were changed similarly at 30° and 22°C were classified as diet dependent. Last, those metabolites altered at 30° and 22°C, but with an opposite trend, were classified as diet and temperature dependent (Fig. 2A and fig. S2A).

From a set of 127 statistically significant metabolites, 63 were diet dependent, 54 were temperature dependent, and only 10 were both diet and temperature dependent (fig. S2B). When metabolites

Downloaded from http://stke.sciencemag.org/ on October 29, 2020

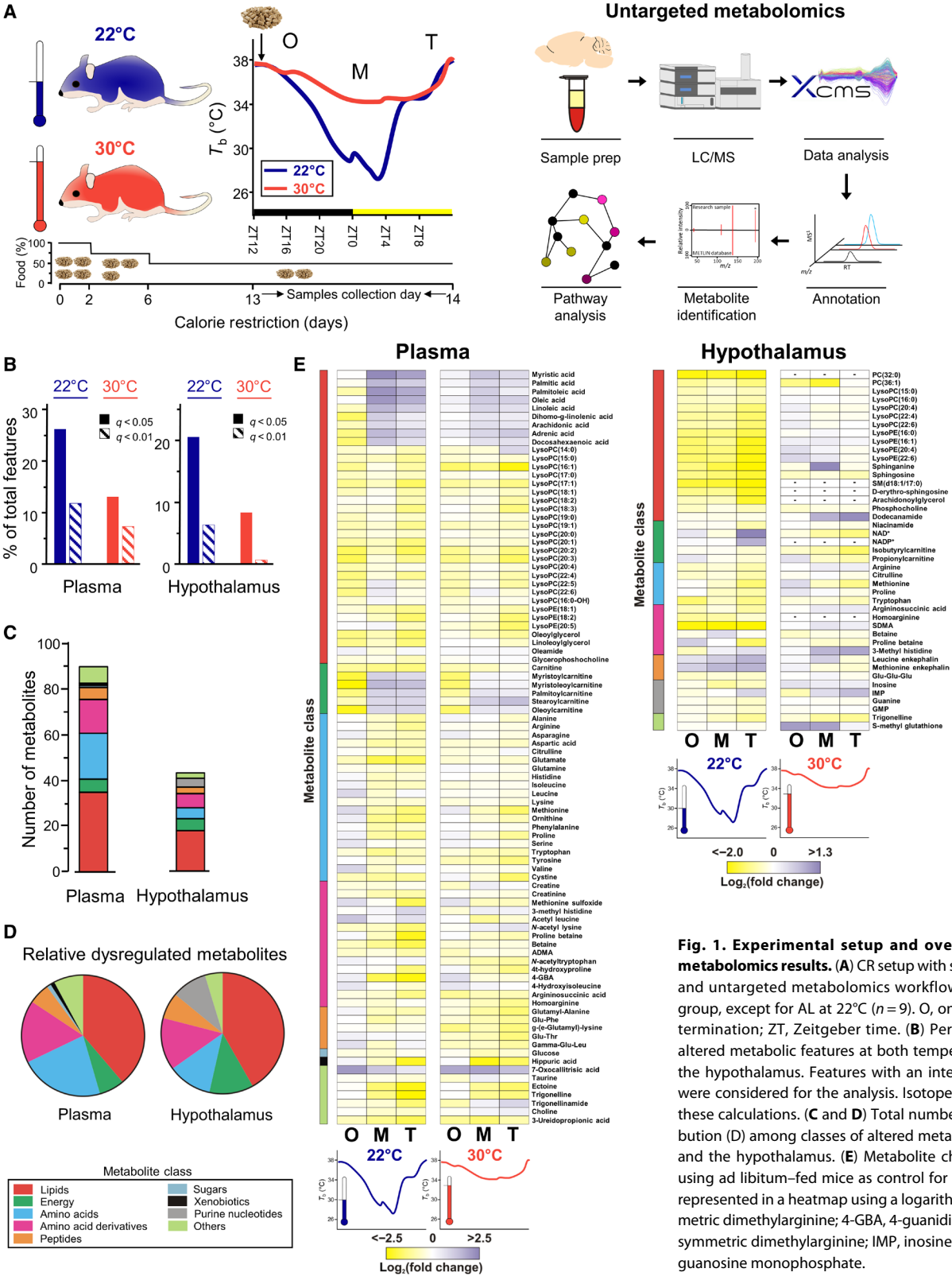

Fig. 1. Experimental setup and overview of untargeted metabolomics results. (**A**) CR setup with sample collection points and untargeted metabolomics workflow. $n = 10$ mice for each group, except for AL at 22°C ($n = 9$). O, onset; M, maintenance; T, termination; ZT, Zeitgeber time. (**B**) Percentage of statistically altered metabolic features at both temperatures for plasma and the hypothalamus. Features with an intensity over 5000 counts were considered for the analysis. Isotopes were removed before these calculations. (**C** and **D**) Total number (C) and relative distribution (D) among classes of altered metabolites found in plasma and the hypothalamus. (**E**) Metabolite changes were calculated using ad libitum–fed mice as control for both temperatures and represented in a heatmap using a logarithmic scale. ADMA, asymmetric dimethylarginine; 4-GBA, 4-guanidinobutanoic acid; SDMA, symmetric dimethylarginine; IMP, inosine monophosphate; GMP, guanosine monophosphate.

Downloaded from http://stke.sciencemag.org/ on October 29, 2020

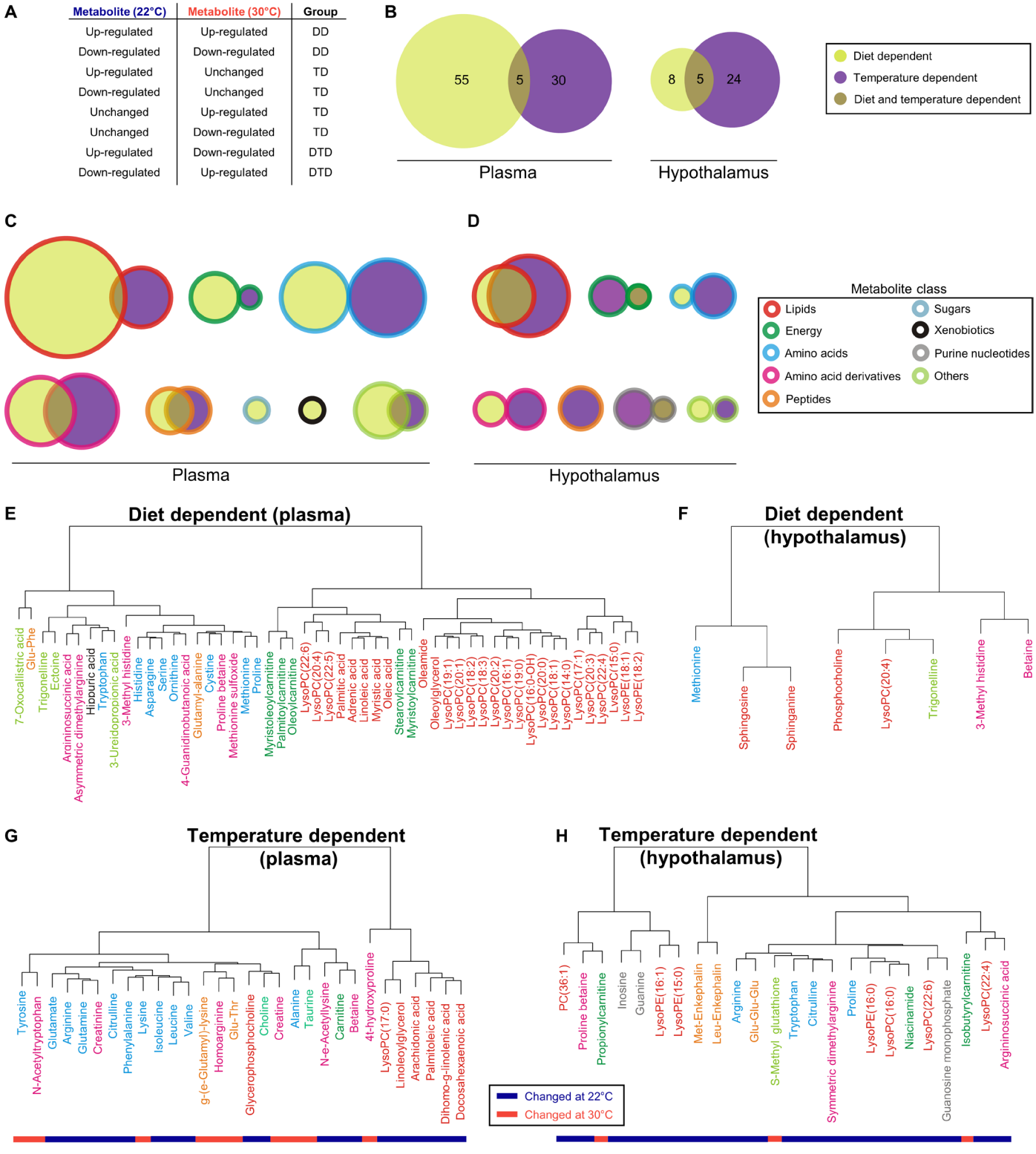

Fig. 2. Classification of metabolites based on the impact of diet or/and temperature. (**A**) Classification of metabolites according to their computational calculated trend during CR. DD, diet dependent; TD, temperature dependent; DTD, diet and temperature dependent. (**B**) Total number of metabolites altered due to diet, temperature, or both in plasma and the hypothalamus. (**C** and **D**) Number of metabolites changed due to food deprivation, temperature, or both by metabolite class in plasma (C) and the hypothalamus (D). Size of circles is proportional to the total number of metabolites of each class. (**E** to **H**) Hierarchical clustering of metabolites sorted in different classes: diet dependent in plasma (E) and the hypothalamus (F) and temperature dependent in plasma (G) and the hypothalamus (H).

Downloaded from http://stke.sciencemag.org/ on October 29, 2020

measured in plasma and the hypothalamus were examined separately, the regulation of plasma metabolites was biased toward diet dependency, whereas the regulation of hypothalamic metabolites was biased toward temperature dependency (Fig. 2B). Fifty-five of 90 plasma metabolites were diet dependent, indicating the influence of food reduction in the systemic response to CR. Still, one-third of the total plasma metabolites were temperature dependent, pointing to the systemic processes that are highly affected by thermoneutrality (Fig. 2B). In contrast, most of the metabolites found in the hypothalamus (24 of 37) were classified as temperature dependent, with only 8 being diet dependent (Fig. 2B).

With the altered metabolites sorted into groups based on the dominant factor influencing their regulation, we further categorized the metabolites by their chemical classes (Fig. 2, C and D). In mice housed at room temperature, CR primarily affected energy metabolism because 83% of the observed changes were in energy metabolites and 77% were lipids (Fig. 2C). By contrast, thermoneutrality affected predominantly amino acid–related groups (amino acids, amino acid derivatives, and peptides) (Fig. 2C). In the hypothalamus, temperature played a greater role than diet in regulating all metabolite classes, and the regulatory contribution of diet was notable only for lipids (Fig. 2D).

To extract information about the global regulation of metabolites sorted in different groups, hierarchical clustering analyses were carried out, based on similarity of the metabolic regulatory trends over the course of the CR. In plasma diet-dependent metabolites, two main clusters were formed. One main cluster contained all lipids and acylcarnitines, whereas the other contained amino acids and amino acid derivatives, suggesting a global regulation of the lipid-energy axis and of certain amino acid metabolism pathways during CR (Fig. 2E). Only eight hypothalamic metabolites were diet dependent. In the hierarchical clustering, sphinganine and sphingosine, the two main sphingoid bases (*30*), grouped together with a strong linear correlation (Fig. 2F and fig. S2C). This similar response could indicate that the entirety of sphingolipid metabolism is changed during CR, which was predicted in our pathway enrichment analysis (data file S3).

Temperature-dependent plasma metabolites formed two main clusters (Fig. 2G). One branch was mainly composed of lipids, namely, free fatty acids (FFAs), which changed in abundance during CR at 22°C only (Fig. 2G). The other cluster mainly contained various amino acids and amino acid derivatives. Most amino acids grouped together. The three branched-chain amino acids (BCAAs) leucine, isoleucine, and valine clustered next to each other (Fig. 2G). This similar response of the BCAAs to CR, based on clustering location and a strong linear correlation (fig. S2C), suggests a regulated systemic metabolism of BCAA upon CR that depends on thermoneutrality (fig. S2D).

In the clustering of temperature-dependent hypothalamus metabolites, the four amino acids measured (arginine, tryptophan, citrulline, and proline) grouped in close proximity (Fig. 2H). Because purine metabolism was predicted to be altered in the hypothalamus by our pathway analysis (data file S3), the presence of three purine metabolites as temperature dependent suggests that this pathway activation during CR is influenced by T_a.

Last, five metabolites in each tissue were classified as diet and temperature dependent. This group of metabolites was characterized by alteration at both T_a but in opposite directions (fig. S2E). Overall, the temperature-dependent metabolites and pathways identified in this study using untargeted metabolomics technologies are molecules that may directly mediate hypothermia during CR and/or regulate the beneficial physiological consequences of CR.

Systemic response to CR in animals housed at 22°C or at 30°C

Changes observed in plasma can be considered an index of the systemic responses to CR. On the other hand, because the hypothalamus regulates nutrient and temperature homeostasis, it not only is subject to the effects of CR but also coordinates the physiological responses to it. Thus, to gain insight into the tissue specificity and the integrative response to CR, we measured the intra- and the intertissue correlation of the metabolites altered at 22° or 30°C.

All plasma and hypothalamic metabolites were plotted in correlation networks that connected all metabolites with a Pearson correlation coefficient of $|\rho| > 0.6$. Correlations between two metabolites were found within the same tissue (intraplasma or intrahypothalamus) and across the tissues investigated (intertissue correlation between plasma and hypothalamus) (Fig. 3A). Mice housed at room temperature showed a total of 1022 correlations, of which 759 (~74%) were intraplasma, 175 (~17%) were intrahypothalamus, and 88 (~9%) were between plasma and hypothalamus. Thermoneutrality reduced the number of correlations by nearly half to a total of 465, of which 405 (~87%) were intraplasma, 175 (~11.7%) were interhypothalamus, and only 6 (~1.3%) were between plasma and hypothalamus (Fig. 3A).

To elucidate how different metabolites and pathways were coordinated in response to CR, the number of correlations per metabolite class was calculated (data file S4) and plotted as chord diagrams. In plasma, the most common intratissue correlations at both T_a were lipid-lipid connections, and their number at thermoneutrality was ~50% of that at 22°C (Fig. 3B). A similar scenario was found for the number of lipid-energy metabolite correlations that, at 30°C, was only ~25% of that seen at room temperature (Fig. 3B). Thermoneutrality also reduced the amino acid–amino acid and amino acid–amino acid derivative correlations found in the plasma of mice housed at 22°C by ~75 and ~78%, respectively (Fig. 3B). With only a few exceptions (lipid-peptide), all correlations between different metabolite classes in plasma were diminished when mice were housed at thermoneutrality (Fig. 3B). The effects of thermoneutrality on the number of intratissue correlations in the hypothalamus were particularly strong for lipid–amino acid and lipid–amino acid derivatives, which were reduced by ~97 and ~100% compared to those found at 22°C, respectively (Fig. 3C). Similarly, thermoneutrality reduced most of the correlations observed between a metabolite in plasma and a metabolite in the hypothalamus, generally lipids and amino acid–related metabolites (Fig. 3D and fig. S3). The interaction between lipid and amino acid metabolism coordinates the response to food reduction during CR at room temperature (*31*). Our data suggest that such response depends on T_a and is nearly abolished at thermoneutrality.

These data indicate that thermoneutrality impinged on both the intra- and intertissue correlations by reducing their number. The effects were particularly strong on the intertissue correlation, suggesting that a portion of the changes occurring in the hypothalamus in response to CR may contribute to the systemic physiological response to CR.

Energy expenditure and fuel usage during CR

Thermoneutrality prevents heat loss and affects energy homeostasis by eliminating the cost associated with the maintenance of constant T_b. Thus, endotherms housed at thermoneutrality have reduced energy expenditure. This was evident when comparing animals fed AL and housed at 22° or 30°C (Fig. 4A and data file S10). Eventually, differences

Downloaded from http://stke.sciencemag.org/ on October 29, 2020

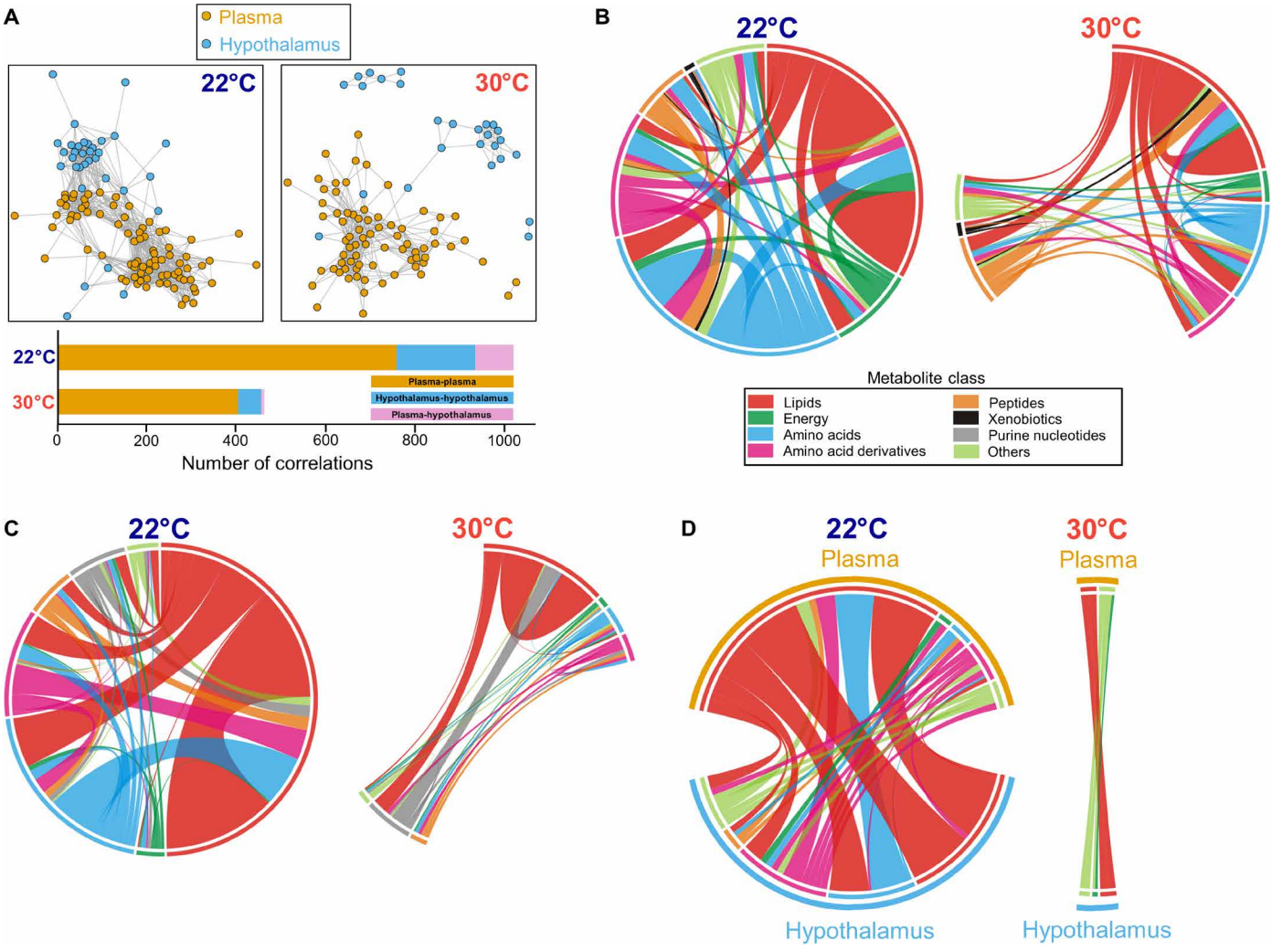

Fig. 3. Effect of thermoneutrality on intra- and intertissue correlation. (**A**) Correlation networks of metabolites at 22° and 30°C and their quantitation. A connection is established between either two metabolites of plasma or hypothalamus when their Pearson correlation coefficient is higher than 0.6 in absolute value. (**B** and **C**) Intratissue correlation of metabolites by class in plasma (B) and the hypothalamus (C) at 22° and 30°C. The length of the circular arc is proportional to the total number of correlations for each class of metabolite and ribbon thickness is proportional to the number of metabolites correlated between two classes of metabolites. (**D**) Intertissue correlations between metabolites in plasma and the hypothalamus classified by metabolite class at 22°C. The length of the circular arc is proportional to the total number of correlations for each class of metabolite and ribbon thickness is proportional to the number of metabolites correlated between two classes of metabolites. $n = 10$ mice for each group, except for AL at 22°C ($n = 9$) for (A) to (D). All 90 plasma metabolites and 37 hypothalamic metabolites were used to compute the correlations [all metabolites found except those hypothalamic metabolites that were measured at 22°C, but could not be found at 30°C: PC(32:0), SM(d18:1/17:0), erythro-sphingosine, arachidonoylglycerol, $NADP^+$, and homoarginine]. The number of samples used to calculate the correlation between any two metabolites was the same (39 samples at 22°C and 40 samples at 30°C).

in energy expenditure were reduced in mice on CR because animals housed at 22°C developed hypothermic responses and gradually lowered their energy expenditure (Fig. 4A and data file S10). By day 8, when samples were collected for the metabolomics analyses, these differences were marginal (Fig. 4A and data file S10). Thermoneutrality also affected the respiratory exchange ratio (RER) (Fig. 4B), an indirect index of the relative utilization of lipids or carbohydrates as source of energy. RER was higher at thermoneutrality, indicating that mice housed at 30°C used a higher ratio of carbohydrates than those housed at 22°C, which used mostly lipids. At day 8 of CR, this difference was also statistically significant (Fig. 4B and data file S9).

This result was consistent with several of our metabolomics findings that also showed specific differences to the phase of the hypothermic response. Lipolysis is one of the first responses to CR (*9*). It increases the availability of FFAs in plasma to provide substrates for β-oxidation in peripheral organs and tissues. CR elevated total FFAs in the plasma but did so more (twofold difference) in mice housed at room temperature than at thermoneutrality (Fig. 4C). The level of FFAs was the highest when hypothermia was maximal in animals at 22°C and to the corresponding time point in animals at 30°C. Once generated, FFAs are converted into acylcarnitines to be shuttled into the mitochondria. The profile of total plasma acylcarnitines, as well as that of four of the total five individual acylcarnitines

Downloaded from http://stke.sciencemag.org/ on October 29, 2020

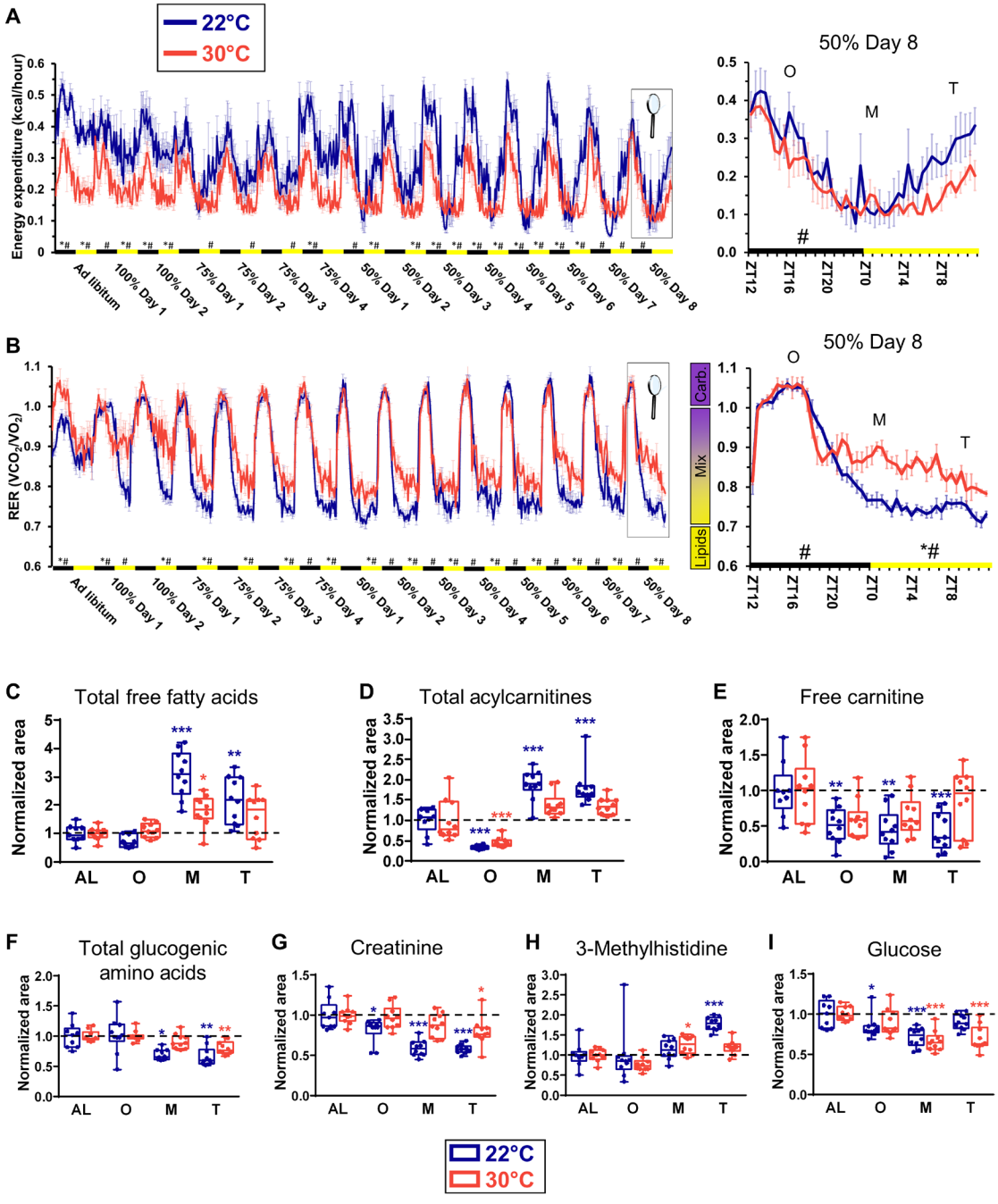

Fig. 4. Temperature dictates fuel use and energy expenditure during CR. (**A**) Energy expenditure of mice recorded every 30 min. Data at day 8 of CR with 50% of food (samples collection) is enlarged. $n = 6$ mice for mice at 22°C and $n = 4$ mice at 30°C. (**B**) Fuel use of mice measured by indirect calorimetry during the course of the CR. The respiratory exchange ratio (RER) was recorded every 30 min. RER > 1.0 indicates an exclusive use of carbohydrates as fuel; RER < 0.7 indicates an exclusive use of lipids as fuel; and 0.7 < RER < 1.0 indicates a mixed use of carbohydrates and lipids as source of energy. Data at day 8 of CR with 50% of food (samples collection) is enlarged. $n = 6$ mice for mice at 22°C and $n = 4$ mice at 30°C. (**C**) Total free fatty acids in plasma calculated as the weighted sum of all free fatty acids. (**D**) Total acylcarnitines in plasma calculated as the weighted sum of all acylcarnitines. (**E**) Free carnitine levels measured in plasma. (**F**) Total glucogenic amino acids in plasma calculated as the weighted sum of all glucogenic amino acids found in the datasets (Ala, Arg, Asn, Asp, Glu, Gln, His, Met, Pro, Ser, Val, Ile, Phe, Trp, and Tyr; see data file S5). (**G**) Creatinine levels in plasma. (**H**) 3-Methylhistidine levels in plasma. (**I**) Glucose levels in plasma. $n = 10$ mice for each group, except for AL at 22°C ($n = 9$) for (C) to (I). For statistical comparisons in (A) and (B), data were grouped by day and activity period, establishing the activity (light off, ZT12-23, black rectangles) and sleeping periods (lights on, ZT0-12, yellow rectangles) as whole units for statistical analysis. Repeated measures two-way ANOVA followed by Bonferroni's multiple comparison correction was used to analyze differences between T_a groups on RER and energy expenditure. *$P < 0.05$, two-way ANOVA means are significantly different; #$P < 0.05$, significant difference between specific time points determined by Bonferroni's multiple comparison test. In (C) to (I), data were normalized using the ad libitum (AL) values as reference for both temperatures. Data were presented as box-and-whisker plots showing the data from all mice analyzed. Outliers were not removed. *$P < 0.05$; **$P < 0.01$; ***$P < 0.001$ determined by a one-way ANOVA followed by a Tukey's HSD test, using AL data as reference for O, M, and T time points.

Downloaded from http://stke.sciencemag.org/ on October 29, 2020

measured, was similar to that of FFAs (Fig. 4D and fig. S4A). Free carnitine, a necessary substrate for the synthesis of acylcarnitines from FFAs, was decreased during CR more so in mice housed at room temperature than in mice housed at thermoneutrality (Fig. 4E). Overall, global untargeted metabolomics results unveiled a high degree of dependence on T_b of the main products of lipolysis during CR, suggesting that thermoneutrality is a relevant factor for lipid and energy metabolism of animals during adaptation to CR.

Gluconeogenesis from free amino acids has been described as a mechanism to maintain glucose levels in models of CR (*31*, *32*). We evaluated the abundance of amino acids in response to CR. We found that up to 15 glucogenic amino acids were altered in the plasma (data file S5). Pathway analysis also predicted several biochemical pathways involving amino acid metabolism dysregulated during CR (data file S3). The total amount of glucogenic amino acids was also calculated (Fig. 4F and data file S5). CR decreased the level of glucogenic amino acids in plasma, a trend that might explain the activation of gluconeogenesis (*31*, *33*). However, these changes were greater in animals housed at 22°C than in mice housed at thermoneutrality. At thermoneutrality, changes in total glucogenic amino acids were only statistically significant at the termination phase (Fig. 4F).

CR increases protein turnover [reviewed in (*34*)]. Here, we found that the plasma level of creatinine, an index of muscle mass (*35*), decreased during CR (Fig. 4G). Consistently, plasma 3-methylhistidine, an index of muscle protein turnover (*36*), was slightly elevated by CR toward the end of the hypothermic phase (Fig. 4H). Changes in creatinine and 3-methylhistidine were larger in animals housed at 22°C (Fig. 4, G and H).

The plasma level of glucose was also altered during CR and was at both T_as (Fig. 4I). It decreased at the onset of the hypothermic response (3 hours after feeding) in a similar way for animals housed at 22° and 30°C. This decrease corresponded with the barely altered levels of total glucogenic amino acids, creatinine, and 3-methylhistidine at onset (Fig. 4, F to I). Blood glucose continued to drop during the maintenance of CR for both housing temperatures before increasing toward the AL levels at the termination phase. Recovery of the original AL glucose values was higher in mice housed at room temperature (Fig. 4I).

Overall, these data show that thermoneutrality alters the effects of CR on energy expenditure and fuel use. These changes could be a consequence of the different physical activity of mice at both housing temperatures. However, even when locomotor activity oscillated during daily cycles, the total amount of physical activity for mice in both housing temperatures was nearly identical (fig. S4B and data file S8).

Cognitive computing-guided prioritization of hypothalamic active metabolites

Our previous data showed that during CR, thermoneutrality altered T_b, energy expenditure, fuel usage, and certain metabolites. Because thermoneutrality antagonizes the effects of CR in several models of disease (*23*), some of these metabolites and their pathways may represent targets for mimicking CR, but their validation will require extensive and expensive survival studies. Instead, other pathways may contribute to the physiological changes caused by thermoneutrality. Among these, there may be molecules that modulate the hypothermic response to CR, a more accessible parameter for validation. We searched for such molecules among the metabolites identified in the hypothalamus. This brain region controls nutrient and temperature homeostasis and was greatly affected by thermoneutrality (>78% of the metabolites changed due to CR were altered by thermoneutrality). We used cognitive accelerated literature mining to rank hypothalamic metabolites according to their known and predicted literature-based relationships with biological processes, in this case temperature control by the hypothalamus (*27*). This artificial intelligence platform uses natural language processing (NLP) to interpret the text of more than 25 million MEDLINE abstracts and to rank literature-based predicted relationships between the metabolites, candidates to be ranked, and specified biological conditions (Fig. 5A) (*27*).

The analysis revealed that methionine enkephalin (MetEnk) and its structurally related molecule LeuEnk were the top 2 ranked metabolites (Fig. 5B and data file S6). These results were validated by rerunning the analysis with all possible combinations of three of the total five known biological entities, obtaining the same results (fig. S5A). In addition, to avoid a biased prioritization based on literature search only, two scores based on metabolite statistical analysis and fold change during CR at both temperatures were introduced. These scores prioritized those metabolites that changed upon CR at 22°C (when mice enter in hypothermia) and those that remained invariant at thermoneutrality (fig. S5B). If these three ranking methods were weighted equally, MetEnk remained the top ranked compound, whereas LeuEnk dropped to fifth place (Fig. 5C). Overall, these metabolites represent good candidates for endogenous modulators of temperature during CR (temperature mimetics), based on the NLP cognitive search.

LeuEnk and MetEnk levels increased during CR in hypothermic mice but remained unchanged at thermoneutrality (Fig. 5D), a behavior that was not mimicked by any other metabolite in the hypothalamus (Fig. 1E). Because these peptides are opioid neurotransmitters that contribute to regulate metabolic responses (*37*, *38*), we hypothesized that they could modulate the hypothermic responses during CR. Activation of the δ opioid receptor by the synthetic LeuEnk analog [D-Ala^2, D-Leu^5]-enkephalin increases body temperature under normal feeding when injected into the hypothalamus (*39*). Intracerebroventricular administration of LeuEnk modified T_b in AL-fed mice (Fig. 5E) and allowed the identification of a related signaling pathway that modulates hypothermia, energy expenditure, and body weight in mice (*40*). These results indicate the value of cognitive computing-guided prioritization of endogenous metabolites to streamline discovery of active metabolites controlling temperature and raises the possibility for the validation of other metabolites on that list as temperature or CR mimetics or even lifespan enhancers.

Role of the citrulline-NO cycle in the hypothermic response to CR

Arginine and its structurally and functionally related metabolite symmetric dimethylarginine (SDMA) (*41*, *42*) were ranked among the top 3 metabolites that might regulate temperature in the hypothalamus (Fig. 5C). Moreover, CR altered several of the metabolites in the urea cycle in both the hypothalamus and plasma, as revealed by pathway analysis (Fig. 6A and fig. S6A). Changes in the urea cycle were focused on the metabolites that belong to the citrulline-NO cycle: arginine, argininosuccinic acid, and citrulline (Fig. 6A, green dashed area). The citrulline-NO cycle is characterized by the synthesis of NO and citrulline from arginine by the NO synthases (NOS), using NADPH [reduced form of nicotinamide adenine dinucleotide phosphate ($NADP^+$)] as cofactor. Citrulline may be recycled back to arginine, using argininosuccinic acid as an intermediate product

Downloaded from http://stke.sciencemag.org/ on October 29, 2020

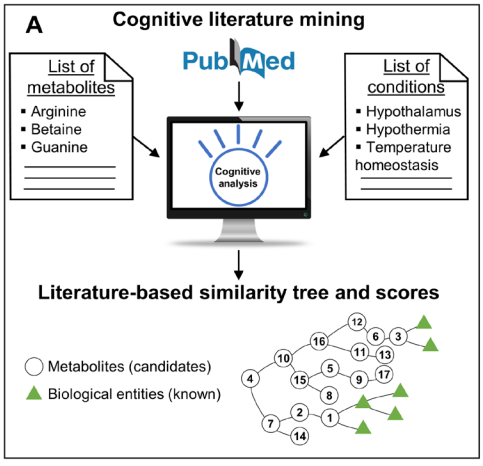

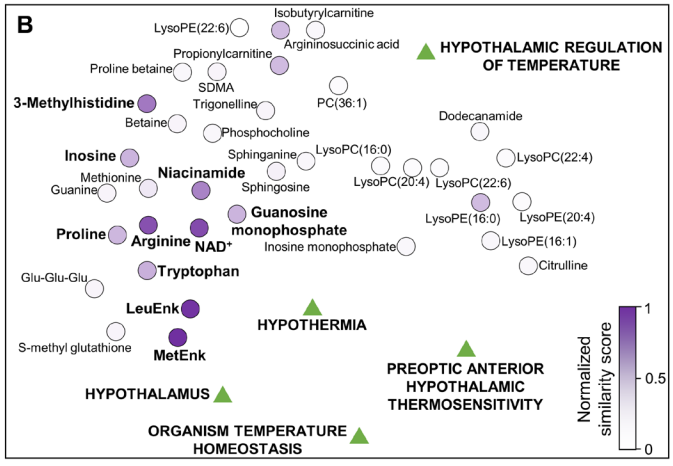

Metabolite	Score
MetEnk	1.00
LeuEnk	0.98
NAD+	0.87
Arginine	0.84
3-Methyl-histidine	0.65
Niacinamid e	0.60
Tryptophan	0.38
Guanosine monophos-phate	0.36
Inosine	0.36
Proline	0.35

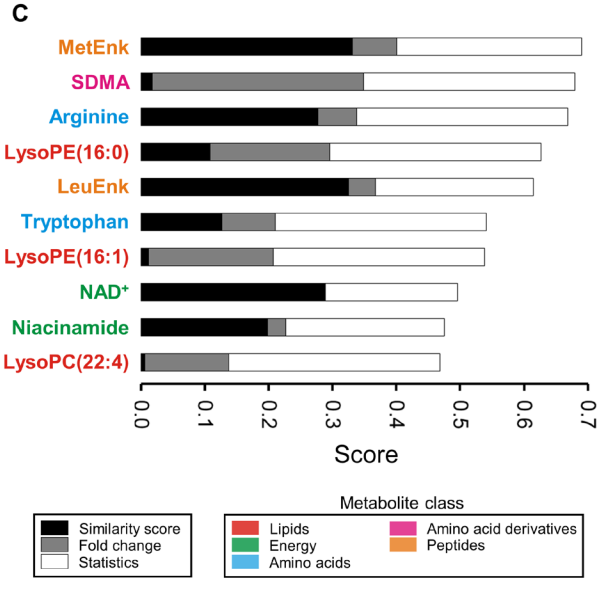

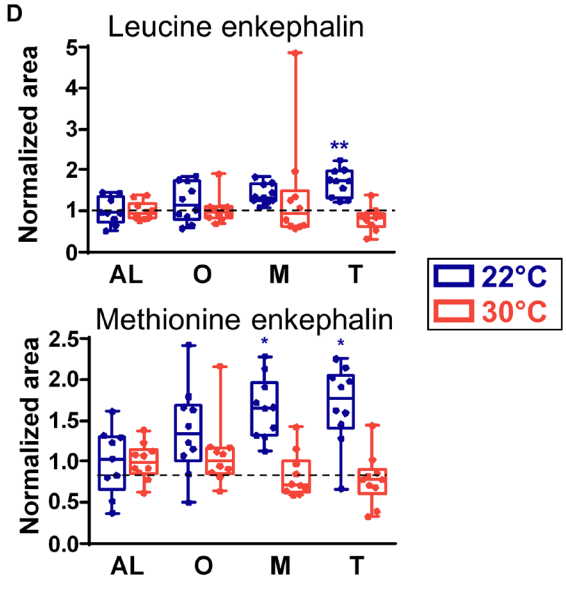

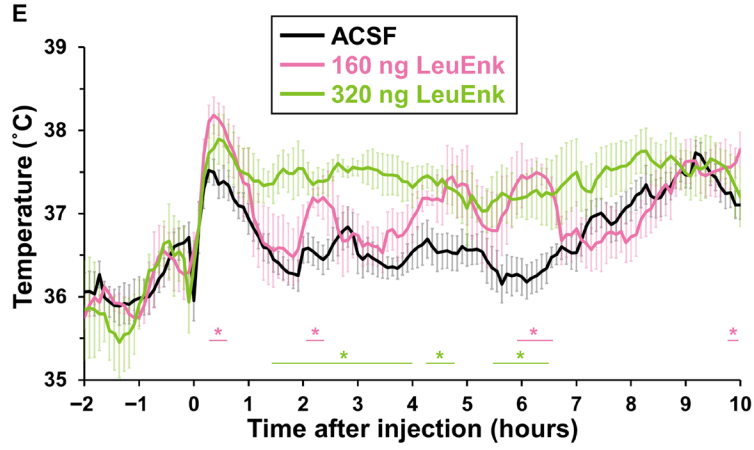

Fig. 5. Cognitive computing-guided prioritization of hypothalamic metabolites. (**A**) The cognitive predictive analysis used NLP of scientific literature to find relationships between candidate metabolites and known biological conditions, ranking metabolites attending to the number of literature-based connections. (**B**) Distance network of known biological conditions and candidate metabolites are depicted as a function of the literature-based relationships found between them, calculated in the similarity matrix. MEDLINE abstracts were used to search relationships. The closer a metabolite is to the biological conditions, the higher is the rank. The normalized similarity score is plotted as a heatmap. LysoPC(15:0) was not ranked because no documents were found. (**C**) Two more rankings based on metabolite statistics and fold change during CR for both temperatures. The similarity score was averaged with these two scores. (**D**) Leucine enkephalin and methionine enkephalin levels measured in the hypothalamus. $n = 10$ mice for each group, except for AL at 22°C ($n = 9$). (**E**) T_b profile of C57BL6 mice upon intracerebroventricular administration of multiple doses of leucine enkephalin or vehicle (artificial cerebrospinal fluid) during ad libitum feeding at time 0. $n = 4$ mice for each group. Data in (D) were normalized using the ad libitum (AL) values as reference for both temperatures. Data were presented as box-and-whisker plots showing the data from all mice analyzed. Outliers were not removed. $^*P < 0.05$ and $^{**}P < 0.01$ determined by a one-way ANOVA model by Tukey's HSD test, using AL data as reference for O, M, and T time points. In (E), $^*P < 0.05$, determined by repeated measures two-way ANOVA followed by Bonferroni's multiple comparison test.

Downloaded from http://stke.sciencemag.org/ on October 29, 2020

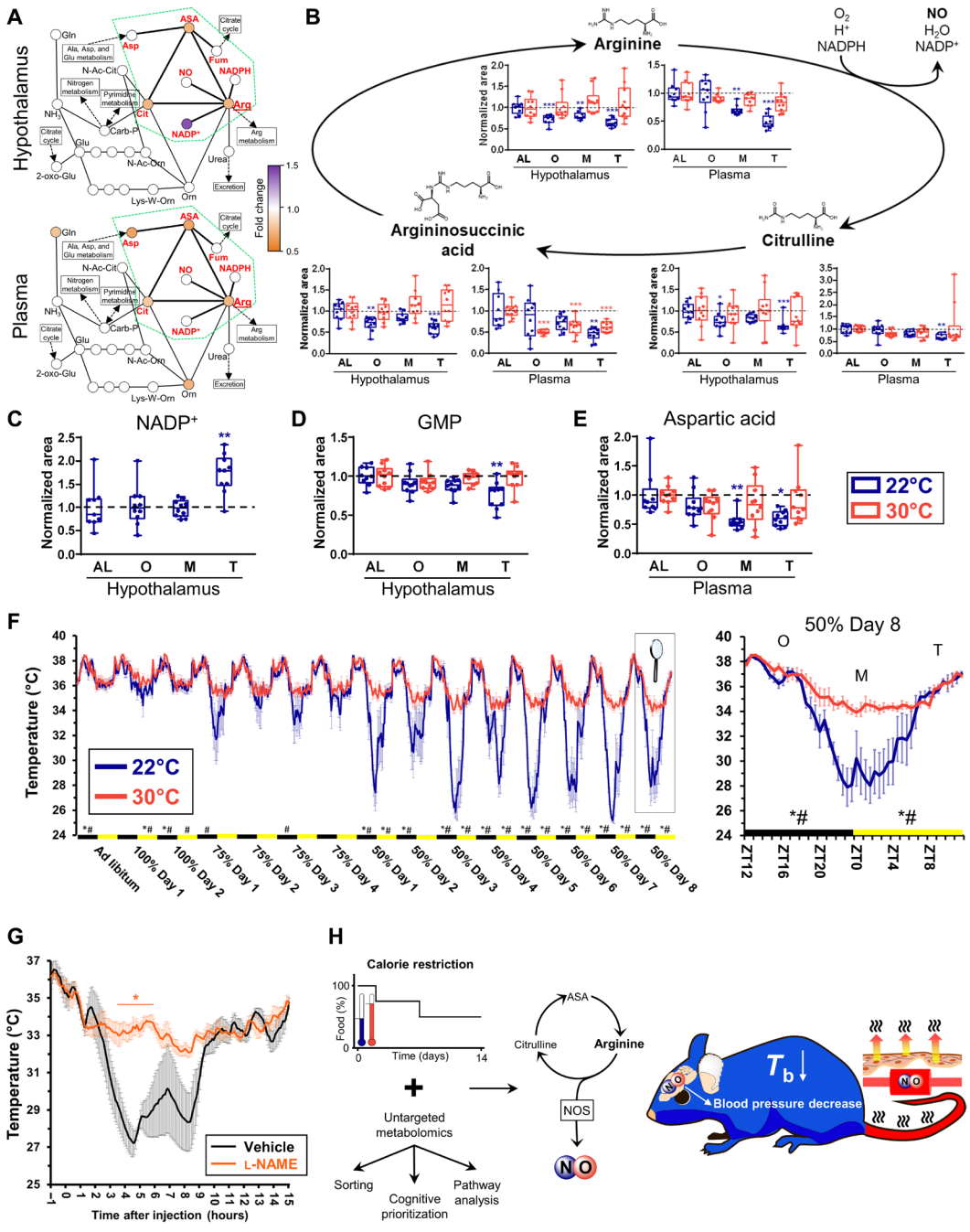

Fig. 6. The citrulline-NO cycle plays a pivotal role in the hypothermic response to CR. (**A**) Several metabolites of the urea cycle are altered following CR in both the hypothalamus and plasma, especially those of the citrulline-NO cycle (contained within the green dashed area). Fold change shown corresponds to an average of O, M, and T data compared to AL at 22°C. (**B**) Citrulline-NO cycle main metabolites measured in the hypothalamus and plasma. (**C**) $NADP^+$ levels in the hypothalamus. (**D**) Guanosine monophosphate levels in the hypothalamus. (**E**) Aspartic acid levels measured in plasma. $n = 10$ mice for each group, except for AL at 22°C ($n = 9$) for (B) to (E). (**F**) Core body temperature was continuously recorded by a rectal temperature probe. Data at day 8 of CR with 50% of food (samples collection) is enlarged. $n = 6$ mice for mice at 22°C and $n = 4$ mice at 30°C. (**G**) Pharmacological inhibition of NOS during CR. Temperature profile of C57BL6 mice on 50% CR was measured after subcutaneous injection of L-NAME (50 mg/kg) (N^G-nitro-L-arginine methyl ester) or vehicle. Injections were performed at time 0, which is 5 to 6 hours before the hypothermic response starts (ZT18 to ZT19). Both mice injected with vehicle and L-NAME ate the full amount of food provided during a 1-hour window starting at ZT12. $n = 4$ mice for vehicle, $n = 5$ mice for L-NAME. (**H**) Proposed model. CR activates the citrulline-NO cycle to generate NO at both the local and systemic levels, helping mice housed at room temperature to lose heat and enter in hypothermia. In (B) to (E), data were normalized using the ad libitum (AL) values as reference for both temperatures. Data were presented as box-and-whisker plots showing the data from all mice analyzed. Outliers were not removed. $^*P < 0.05$; $^{**}P < 0.01$; $^{***}P < 0.001$ determined by a one-way ANOVA model by a Tukey's HSD test, using AL data as reference for O, M, and T time points. For statistical comparisons, data in (F) were grouped by day and activity period, establishing the activity (light off, ZT12-23, black rectangles) and sleeping periods (lights on, ZT0-12, yellow rectangles) as whole units for statistical analysis. Repeated measures two-way ANOVA followed by Bonferroni's multiple comparison correction was used to analyze differences between T_a groups on RER and energy expenditure. $^*P < 0.05$, two-way ANOVA means are significantly different; $\#P < 0.05$, significant difference between specific time points determined by Bonferroni's multiple comparison test. In (G), $^*P < 0.05$, determined by repeated measures two-way ANOVA followed by Bonferroni's multiple comparison test.

(Fig. 6B) (*41*). In the hypothalamus, metabolites of the citrulline-NO cycle decreased over the 24-hour course of CR in mice housed at 22°C compared to mice fed AL (Fig. 6B), indicating a coordinated activation of this pathway in the hypothalamic response to CR for mice at 22°C. However, the three metabolites remained unaltered when mice were housed at thermoneutrality (Fig. 6B). In addition, $NADP^+$, a cofactor produced together with NO in the conversion of arginine into citrulline, was up-regulated during CR-induced hypothermia (Fig. 6C), suggesting that NO synthesis may also be activated. One function of NO is activating guanylate cyclase to promote the synthesis of cyclic guanosine 5′-monophosphate (cGMP) from GMP (*43*, *44*). GMP levels decreased in the hypothalamus of mice housed at 22°C, indicating that cGMP synthesis was activated. In contrast, GMP levels remained unaltered in mice at thermoneutrality (Fig. 6D).

Downloaded from http://stke.sciencemag.org/ on October 29, 2020

Similar changes in arginine and citrulline were seen in the plasma, although argininosuccinic acid also decreased at thermoneutrality, suggesting that it might have been used to maintain arginine levels (Fig. 6B). Aspartic acid, a substrate for the recycling of citrulline (Fig. 6A), was lower in mice housed at 22°C than at 30°C (Fig. 6E). Last, other metabolites structurally and functionally related to arginine, such as SDMA and homoarginine (*41*, *43*), were dysregulated in plasma and the hypothalamus (fig. S6B).

NO is a gaseous substance that contributes to both central and peripheral thermoregulation (*39*, *41*). Thus, we hypothesized that a mechanism by which CR lowers T_b (Fig. 6F) is by stimulating the synthesis of NO and sought to test this hypothesis pharmacologically. Mice housed at room temperature were injected subcutaneously with the nonselective NOS inhibitor L-NAME (N^G-nitro-L-arginine methyl ester) or vehicle before CR-induced hypothermia. L-NAME prevented CR-induced hypothermia (Fig. 6G) to a similar extent as thermoneutral housing (Fig. 6F). These data indicate that NO is engaged in the regulation of hypothermia during CR. This also helps to validate our cognitive computing approach in the identification of active metabolites in the changes during CR and thermoneutrality.

The citrulline-NO cycle is closely related to the urea cycle and polyamine metabolism (fig. S6C). Because spermidine supplementation has been proposed to enhance life span and health span (*45*–*49*), we designed a targeted method to measure this metabolite. We observed that the plasma level of ornithine, but not that of spermidine, was transiently lowered by up to 50% during maintenance and termination phase of CR in animals housed at 22°C or at thermoneutrality (fig. S6C). In contrast, the level of spermidine increased transiently during the maintenance and termination phase of CR (fig. S6C) but remained unchanged during CR in the hypothalamus for both house temperatures. Thus, we observed that temperature influences spermidine metabolism during CR in plasma. Furthermore, we demonstrated that NO synthesis by a coordinated activation of the citrulline-NO cycle contributes to the hypothermic response to CR only in animals housed at room temperature but not at thermoneutrality (Fig. 6H).

DISCUSSION

In this work, we performed untargeted metabolomic analysis to compare the effects of CR in animals housed at two different T_a. One was 22°C, which approximately corresponds to the standard "room temperature" housing conditions at which experiments are typically performed in laboratories across the world. The other was 30°C, a temperature at which most mammals, including mice and humans, are thermoneutral. The rationale for our study is that thermoneutrality exacerbates inflammatory and metabolic disorders (*20*–*22*), prevents the hypothermic response to CR, and antagonizes the beneficial effects that CR has on longevity (*23*).

The 50% CR used here can be considered a model of severe CR. Experiments investigating the beneficial effects of CR on life span typically provide 60% of the AL diet or more. However, such regimens are usually applied for the entire duration of the life-span experiments. Here, we subjected animals to 75% CR (animals received 25% less of the amount of food consumed AL) for 4 days followed by 50% CR for 8 days. The regimen and time points were chosen because a parameter we wanted to investigate was the reduction of core body temperature that occurs during CR at room temperature but not at thermoneutrality, and such a hypothermic response is larger at 50% CR, compared to milder CR regimens. However, in moving forward with the investigation, it will be important to determine if the changes observed here on a 50% CR regimen applied for 8 days are similar to those that may be induced by a milder CR regimen and for longer periods of time.

The data collected using the experimental model proposed here indicate that thermoneutrality greatly affected the metabolome of animals subject to CR. Many such changes can be attributed to differences in core body temperature observed in animals housed at 22°C compared to that in animals at thermoneutrality. However, further work is required to determine the specific factors that may affect the changes observed. Among them is the sex specificity of the metabolomic profile. Data were collected from female animals only because females show changes in core body temperature to CR that are larger than those seen in male mice, as we have described before (*10*, *40*, *50*). Another factor that might contribute to the differences observed is the contribution of the microbiome that can affect both the response to CR as well as the metabolic rate (*51*, *52*). However, plasma metabolomics should have captured most of the changes introduced by the microbiome in our model, and several models that characterize the plasma metabolome use it as a surrogate measure of microbiome changes (*53*, *54*). Last, it will be interesting to determine whether and to which extent the sympathetic nervous system, which regulates physiological thermoregulatory response, may contribute to the differences observed. The autonomic nervous system may play a role in hypothermia through neuronal NOS (nNOS), which is expressed in peripheral nitrergic nerves. Smooth muscle tissues are innervated by nitrergic neurons expressing nNOS, which generates NO, which acts on the surrounding cells by decreasing vascular tone, helping to trigger hypothermia through heat loss (*43*, *55*).

We showed in animals subjected to long-term CR how the prevention of the CR-induced hypothermia facilitates body weight loss by limiting the hypothermic response that reduces energy expenditure (*40*). During the short-term CR used here, body weight was still similar in CR animals housed at room temperature and at thermoneutrality (fig. S1A). In addition, no differences were found in the lean–to–body weight and fat–to–body weight ratio in groups of animals housed at room temperature or at thermoneutrality (fig. S1B). These data, together with the fact that samples were collected 20 hours after the last meal, indicate that the effects of food on the metabolome were minimized and that the experimental setting offered a reasonable platform to investigate the metabolites and pathways associated with temperature. We anticipated that changes in the metabolome may be used to investigate at least two biological functions: pathways that may contribute to the beneficial effects of CR on longevity and those that may be involved in regulating the hypothermic response to CR. The first set of pathways is more likely to be identified by evaluating the changes found in the plasma, which was used as an index of systemic changes. The latter set of pathways could be identified by evaluating changes occurring in the hypothalamus because this brain region is pivotal in regulating temperature homeostasis. In this study, validation was carried out for metabolites involved in the regulation of the hypothermic response to CR.

We found that thermoneutrality reversed 39% of those metabolic changes observed in plasma upon CR and 78% of those in the hypothalamus. In both tissues, these changes were primarily due to amino acids and their derivatives and, to a lesser extent, due to lipids and energy metabolites as demonstrated with the total FFA and acylcarnitine

Downloaded from http://stke.sciencemag.org/ on October 29, 2020

levels (Fig. 4, C and D). One way to interpret these data is by considering that reduced calorie intake triggers the use of stored energy and that such energetic requirement is different in animals housed at distinct T_a, because thermoneutrality reduces the energetic cost required to maintaining a constant T_b (*11*). Thus, the 75% decrease in lipid-energy metabolite correlations in plasma at thermoneutrality is a likely indication that mice at 30°C do not need as much acylcarnitines as mice at 22°C to produce energy through β-oxidation (Fig. 3B). The alteration in amino acids can, in part, also be interpreted in terms of energy requirements because gluconeogenesis from free amino acids mainly in the liver has been described as a mechanism to maintain glucose levels during CR (*31*, *32*). Plasma glucogenic amino acids may be shuttled to the liver and/or other glucogenic organs to be converted into the different intermediates of gluconeogenesis, potentially explaining that decrease in plasma during CR regulates energy balance. In addition, prolonged dietary restriction can activate protein catabolism in muscles, increasing the level of circulating free amino acids, which can be used as an alternative source of energy for gluconeogenesis (*56*). Markers of muscle catabolism were higher at 22°C (Fig. 4, G and H).

Amino acid levels during CR may not only mirror metabolic requirements but also exert other contributions to the beneficial effects of CR and are potential candidates for CR mimetics [reviewed in (*57*)]. For instance, reduction of the dietary intake of BCAAs is sufficient to improve glucose tolerance, cardiometabolic health, aging, and longevity (*58*, *59*). Conversely, BCAA supplementation increases body weight and fat mass, promotes insulin resistance, and induces the expression of proinflammatory genes (*60*). We found that the response of the three BCAAs to CR was similar and blunted by thermoneutrality (fig. S2, C and D), indicating how this approach can help to identify endogenous molecules that modulate pivotal phenotypic responses.

Artificial intelligence technology was incorporated to streamline the discovery and development of temperature mimetics for increasing health span, as was demonstrated with LeuEnk (Fig. 5, A to C) and validated in a separate study (*40*). In addition, arginine and SDMA played a role in hypothermia during CR. Lysophospholipids, many of them ranked in the top 15 of the cognitive-driven prioritization (data file S6), are endogenous ligands of the transient receptor potential M8 (TRPM8) (*61*). Activation of TRPM8 in the central nervous system triggers certain physiological responses leading to heat generation, which maintains thermoregulation when body temperature is low. Conversely, blocking TRPM8 leads to physiological responses resulting in body heat dissipation (*62*). In summary, the incorporation of cognitive prioritization strategies on top of untargeted metabolomics results streamlines the assignment of biological activity to altered endogenous molecules, as has been demonstrated for other models of disease (*26*, *63*).

Cognitive-guided prioritization of metabolites, together with pathway analysis, led us to hypothesize that the citrulline-NO pathway metabolites could play an active role in the hypothermic response to CR. We confirmed our hypothesis pharmacologically by showing that inhibition of NOS blocked CR-induced hypothermia. CR affected components of the citrulline-NO cycle in both plasma and the hypothalamus, indicating that NO might regulate temperature during CR by acting both centrally and peripherally. Because the inhibitor used crosses the blood-brain barrier and inhibits eNOS and nNOS, both might contribute to hypothermic responses. However, whether L-NAME subcutaneous administration has other side effects unrelated to the observed changes in the citrulline-NO cycle is yet to be explored in this model. In addition, untargeted analysis revealed that other arginine-related metabolites (dimethylarginine and homoarginine) were altered (fig. S6B). These endogenous molecules affect NO metabolism because of their structural similarity with arginine (*41*). Among them, SDMA is of special interest because it was ranked as the second metabolite that could affect temperature in the hypothalamus (Fig. 5C); however, this hypothesis is yet to be confirmed in this model.

Because of its role in life-span extension and health-span improvement (*45*–*49*) and its metabolic connection with the citrulline-NO cycle (fig. S6C), we measured spermidine in plasma and the hypothalamus. At 22°C, we showed that the activation of the citrulline-NO cycle during CR resulted in the synthesis of NO (reflected in the decrease of arginine and citrulline), which helps to trigger hypothermia (Figs. 6, B and G). However, we did not observe changes in spermidine at 22°C. On the other hand, at thermoneutrality, no variation in arginine and citrulline was observed because NO synthesis was not required (Fig. 6B). However, at 30°C, CR elevated the level of spermidine and reduced that of ornithine and argininosuccinic acid in plasma without modifying arginine and citrulline (Fig. 6B and fig. S6C), suggesting the activation of the polyamine pathway during CR at thermoneutrality. Together, these data indicate that T_a determines whether arginine is used to generate NO (22°C) or spermidine (30°C) during CR. However, the biological importance of the increase in endogenous spermidine in our CR model at thermoneutrality remains to be demonstrated.

The changes in arginine, citrulline, argininosuccinic acid, and SDMA in the hypothalamus were significant only in samples from animals housed at 22°C but not in those from animals housed at thermoneutrality. This observation indicates that the absence of a hypothermic response during CR at thermoneutrality not only is a passive phenomenon due to the lack of a temperature gradient between ambient and organismal surface temperatures but also is an active response that includes the lack of activation of the physiological response that would be required to reduce T_b. Thus, the hypothermic response during CR is dependent not only on energy intake but also on information about the environmental temperature, a parameter that ultimately influences energy expenditure. In the future, it will be interesting to investigate whether the biochemical pathways that regulate physiology of the hypothermic response also affect health span and how this may be affected by T_a.

MATERIALS AND METHODS

Mice and husbandry

All procedures were approved by The Scripps Research Institute Institutional Animal Care and Use Committee. Female C57BL/6 mice that were 4 to 5 months old were used for the experiments. Animals were singly caged on a standard 12-hour light/12-hour dark cycle (lights on 11:00 a.m.; ZT12) at a controlled T_a of 22.0° ± 0.5°C or 30.0° ± 0.5°C. Water was available AL during CR experiments. Food (LabDiet 5053 Irradiated PicoLab providing a physiological fuel value of 3.41 kcal/g, 20.0% protein, 52.9% carbohydrates, 10.6% fat, 4.7% crude fiber, and 6.1% ash) was provided AL or restricted during the CR experiments as specified.

CR setup

Four- to 5-month-old female mice regularly fed AL were subjected to CR. CR was carried out providing a percentage of the amount of

Downloaded from http://stke.sciencemag.org/ on October 29, 2020

food consumed during AL diet, which was calculated as an average of the calories consumed by mice during a period of 4 days fed AL. Animals were given 100% of the AL diet for 2 days to habituate them to daily rations of food. They were then given 75% of AL for 4 days and 50% for 4 days. Food was provided daily at a 1-hour window before lights were turned off (ZT12). All animals ate the entire amount of food provided during CR experiments. To identify the metabolic changes that were due to CR or T_b variation, two different litters underwent the same CR protocol, but were housed at room temperature (22°C) and thermoneutrality (30°C).

Collection of tissue

On day 8 of 50% CR, mice were anesthetized through exposure to isoflurane for 3 min and perfusion with saline was performed to remove traces of blood from tissues. Before perfusion, blood from the right atrium was collected in microvette capillary blood 300 EDTA (Kent Scientific Corporation, Torrington, CT). To obtain plasma, blood was centrifuged at 2000*g* at 2°C for 10 min. Supernatants (plasma) were transferred to polypropylene tubes using a Pasteur pipette. Last, samples were flash-frozen in liquid nitrogen for 1 min and stored at −80°C until their analysis by liquid chromatography–mass spectrometry (LC-MS).

The hypothalamus (~3 mm) was collected after perfusion with saline. Dissection was carried out with sterile forceps, scissors, and scalpel. The brain was placed in a brain coronal matrix and a razor blade was placed on the optic chiasm to isolate the first section (anterior hypothalamus); from there, the second blade was placed on the 3-mm mark (generating the posterior hypothalamus). The hypothalamic nucleus was then isolated from the brain slice, placed in polypropylene tubes, flash-frozen, and stored at −80°C until their analysis by LC-MS.

Monitoring of physiological parameters

Core T_b was monitored using a rectal temperature probe for the animals used for the metabolomics analysis or by radiotelemetry for the physiological data presented. Rectal measurements were carried out using RET-3 probes and thermo recorder HH506A (Omega) and were completed within 40 s after first moving the cage to avoid recording thermogenesis due to handling. Radiotelemetry for measuring T_b and locomotor activity was performed using a transmitter (TA10TA-F10; Data Sciences Inc.) surgically implanted into the peritoneal cavity, as previously described (*13*). Animals were allowed a recovery time of 14 days after surgery and 2 days of habituation to the experimental environment before experiments were begun. Data were recorded by placing a cage containing an animal implanted with a radio transmitter on a receiver plate (RPC-1; DataScience Inc.). Data collection and offline analysis were performed using the Dataquest ART software (DataScience Inc.). Energy expenditure and RER were determined by using a computer-controlled open-circuit system (Oxymax System) that is part of an integrated Comprehensive Lab Animal Monitoring System (Columbus Instruments), as previously described (*64*). Body composition during CR was measured during the first hours of the light period using the Echo3-in-1 NMR analyzer (Echo Medical) as previously described by our group (*10*).

Pharmacology

LeuEnk (Tocris Bioscience, Bristol, UK) was dissolved in artificial cerebrospinal fluid for intracerebroventricular administration through a previously placed cannula during AL feeding. A 7-mm, 26-gauge guide cannula and 7.2-mm injector, 33-gauge internal cannula were used. The guide cannula was implanted at the following stereotactic coordinates: third ventricle, posterior to bregma: 0.50 mm, ventral 4.75 mm from the skull, final ventral coordinate 4.95 mm. L-NAME hydrochloride (Tocris, 0655) was dissolved in saline and administered subcutaneously at 50 mg/kg in mice undergoing 50% CR.

Metabolite extraction

For metabolite extraction from plasma, 450 µl of cold acetonitrile/methanol/water (4:4:1, by volume) was added to 50 µl of previously thawed plasma, to reach a final volume of 500 µl of 2:2:1 (acetonitrile/methanol/aqueous, by volume). To precipitate plasma proteins, samples underwent three cycles of freeze/thaw. Each cycle included a flash freezing step in liquid nitrogen for 1 min, vortexing for 30 s, and sonication in an ice-cold bath for 15 min.

For metabolite extraction from the hypothalamus, a section of tissue (10 to 30 mg) was weighed and 0.6 ml of cold methanol/water (4:1, v/v) was added per 10 mg of tissue. Homogenization was performed by adding glass beads to the samples in a homogenizer and samples were sonicated in an ice-cold bath for 10 min. Samples were transferred to another tube and rinsed with additional 200 µl of methanol/water (4:1, v/v).

After these different homogenization protocols for both plasma and the hypothalamus, all samples were incubated at −20°C for 60 min. Last, proteins were pelleted by centrifuging samples at 16,000*g* for 15 min at 4°C. Supernatants containing all metabolites were transferred to another tube and dried down in a vacuum concentrator. Last, dry metabolite extracts were reconstituted with acetonitrile/water (1:1, vol/vol). Metabolite extracts were vortexed for 1 min, sonicated for 15 min, and centrifuged at 16,000*g* and 4°C for 15 min to remove nonsoluble debris. Plasma samples were reconstituted in 100 µl. For hypothalamus samples, the volume of acetonitrile/water was adjusted using the initial mass of tissue used for extraction, to use the same amount of starting material for the untargeted metabolomics analyses. Supernatants were transferred to LC glass vials and stored at −80°C before their analysis by LC-MS.

Untargeted metabolomics

Samples from mice housed at 22° and 30°C were harvested and analyzed by mass spectrometry independently. Metabolites extracted from plasma and the hypothalamus were analyzed by RP and HILIC (*65*). Plasma sample analyses were carried out in a Bruker Impact II quadrupole/time-of-flight (q-ToF) mass spectrometer coupled to a Bruker Elute UHPLC (Bruker, Billerica, MA). Data were acquired over a mass/charge ratio (*m/z*) range of 50 to 1000 Da. The electrospray source conditions were as follows: end plate offset, 500 V; dry gas temperature, 200°C; drying gas, 6 liter/min; nebulizer, 1.6 bar; and capillary voltage, 3500 V. Sodium formate was used for post-run mass calibration. The same mobile phases were used for both RP and HILIC chromatography, consisting of 0.1% formic acid in water (v/v) as phase A and 0.1% formic acid in acetonitrile (v/v) as phase B. The flow through the column in both cases was 150 µl/min. An ACQUITY BEH C18 column (1.0 mm by 100 mm, 1.7 µm, Waters Corporation, Milford, MA) was used for the RP analysis and an ACQUITY BEH Amide column (1.0 mm by 100 mm, 1.7 µm, Waters Corporation, Milford, MA) was used for the HILIC analysis. The gradient for RP chromatography consisted of 99% phase A for 1 min, 1% phase A over 9 min, and held at 1% phase A for an additional

Downloaded from http://stke.sciencemag.org/ on October 29, 2020

3 min. The gradient for HILIC consisted of 1% phase A for 1 min, 35% phase A over 13 min, 60% phase A over 3 min, and held at 60% phase A for an additional 1 min. Data were acquired in positive ion mode. The injection volume was 2 µl. For identification purposes, putative molecules of interest were fragmented at three different collision energies (10, 20, and 40 eV).

Analyses of hypothalamic samples were carried out in a Synapt G2-Si q-ToF mass spectrometer equipped with an online UHPLC (Waters Corporation, Milford, MA). Data were acquired over an *m/z* range of 50 to 1000 Da. The electrospray source conditions were as follows: capillary, +3.00 kV; sampling cone, 40 V; source temperature, 100°C; desolvation temperature, 250°C; desolvation gas flow, 600 liter/hour; and cone gas flow, 50 liter/hour. LeuEnk (*m/z* 556.2771) was used for lock mass correction. For tissue samples, the same solvents and gradients as above were used. However, the flow through the column was 400 µl/min and columns used were as follows: An ACQUITY BEH C18 column (2.1 mm by 100 mm, 1.7 µm, Waters Corporation, Milford, MA) for the RP analysis and an ACQUITY BEH Amide column (2.1 mm by 100 mm, 1.7 µm, Waters Corporation, Milford, MA) for the HILIC analysis. Data were acquired in positive ion mode. The injection volume was 2 µl. For identification purposes, putative molecules of interest were fragmented at three different collision energies (10, 20, and 40 eV).

Mass spectrometry data analysis

Raw LC-MS data were converted to mzXML format using ProteoWizard MS Converter version 3.0.7529 (*66*). The mzXML files were uploaded to XCMS Online for data processing (*67*). Peaks were first detected, aligned across samples, and integrated. Then, features (a set of integrated peaks with a particular *m/z* and retention time) underwent isotope removal and adduct and in-source ion annotation (*28*, *29*). Data were processed using the following parameter settings: centWave for feature detection (Δ *m/z* = 15 parts per million, minimum peak width = 10 s, and maximum peak width = 60 s); obiwarp settings for retention time correction (profStep = 0.5); and parameters for chromatogram alignment, including mzwid = 0.015, minfrac = 0.5, and bw = 5. Last, after the statistical analysis, only features with $q < 0.05$ were selected for identification through MS/MS experiments. To identify these metabolites, the resulting MS/MS spectra were matched against the METLIN database (*68*). For dodecanamide, a metabolite whose MS/MS was not contained in any spectral databases, the analytical standard was synthesized.

Targeted analysis of spermidine

Spermidine was analyzed by Ultra High Performance Liquid Chromatography (UPLC) (Agilent 1290 Series, Santa Clara, CA) using an Agilent HILIC-z column (2.1 mm by 150 mm, 2.7 µM; Agilent Technologies, Santa Clara, CA). The gradient started at 100% phase B, 10% phase B over 20 min, and held at 10% phase B for an additional 2 min before reequilibration (250 µl/min flow rate). The composition of mobile phase A consisted of water with 10 mM ammonium formate and 0.1% formic acid and mobile phase B consisted of acetonitrile/water 9:1 (v/v) with 10 mM ammonium formate and 0.1% formic acid. The injection volume was 5 µl. UPLC was coupled to an Agilent 6495 Series triple quadrupole mass spectrometer (Agilent Technologies, Santa Clara, CA) operated in positive ion multiple reaction monitoring (MRM) mode to monitor a quantitative (146➔72) and qualitative (146➔30) transition. These transitions were retrieved from METLIN MRM (*69*) and instrument parameters were optimized using the spermidine analytical standard. The same analytical standard was used to run a calibration curve for spermidine for quantitation.

Synthesis of dodecanamide (LAURAMIDE)

Lauric acid (0.54 mmol) was dissolved in anhydrous dichloromethane (DCM) and converted to the acid chloride by reaction with thionyl chloride (2.72 mmol) under nitrogen atmosphere. DCM and excess thionyl chloride were removed by rotary evaporation in vacuo, and the remaining acid chloride was subjected to ammonia by addition of ammonium hydroxide solution. The product was extracted by liquid phase extraction with chloroform and purified by flash column chromatography with ethyl acetate and hexane as eluent to give a white solid.

Dodecanamide structure was verified by nuclear proton magnetic resonance (^{1}H NMR) and high-resolution mass spectrometry (HRMS) accurate mass as follows: ^{1}H NMR (600 MHz, CDCl3) δ 5.42 (s, 2H), 2.24 (m, 2H), 1.66 (dd, *J* = 7.2 Hz, 2H), 1.35 to 1.28 (m, 16H), 0.90 (t, *J* = 6.9 Hz, 3H). ^{13}C NMR (150 MHz, CDCl3) δ 175.05, 35.49, 31.45, 29.15, 29.02, 28.89, 28.87 (d, *J* = 1.7 Hz), 28.79, 25.09, 22.23, 13.66. HRMS (ESI), *m/z* calculated for C12H26NO ($[M + H]^+$): 200.2009, found: 200.2013.

Bioinformatics

Hypothalamic metabolites were ranked using IBM Watson for Drug Discovery platform. A list of keywords and entities related to temperature control by the hypothalamus were used as the known set against which candidate metabolites were ranked. The hypothalamic candidate metabolites were inputted and disambiguated into drug or chemical entities, which contain chemical and structural information, common annotations, and known synonyms. MEDLINE abstracts were queried, and the candidate metabolites were given a similarity score and ranked based on similarity to keywords and entities known to be related to temperature control. Results were validated by re-ranking the metabolites against any random three of the five biological entities used as the known set.

Because each metabolite's relative concentration was measured across four time points, we computationally determined the group to which we attribute each statistically significant altered metabolite by using a probability estimation based on the fold changes of each time point. Three normal distributions were created with the same mean centered at 1 and with an SD equal to 0.05 corresponding to the minimum fold change (1.05 or −1.05) for which we consider a metabolite quantitatively altered (fig. S3A). Left and right distributions (colored) were inverted and clipped to zero below and above fold change 1, respectively. These distributions were used to calculate a probability for a certain metabolite to be classified as diet dependent, temperature dependent, or diet and temperature dependent. Distribution 1 corresponded to up-regulated metabolites upon CR, distribution 2 corresponded to unchanged metabolites upon CR, and distribution 3 corresponded to down-regulated metabolites upon CR. Then, if data for a metabolite in animals housed at both 22° and 30°C lay in distribution 1 or 3, that metabolite was sorted as diet dependent. If data for a metabolite in animals housed at one T_a lay in distribution 1 or 3 and data for the same metabolite in animals housed at the other T_a lay in distribution 2, that metabolite was sorted as temperature dependent. Last, if data for a metabolite lay in distribution 1 in animals housed at one T_a and distribution 3 in animals housed at the other T_a, this metabolite was classified as diet and temperature dependent. Because statistical significance was not

Downloaded from http://stke.sciencemag.org/ on October 29, 2020

considered in the classification, we introduced a post hoc factor to correct for false positives. Metabolites classified as distribution 1 or 3 by the algorithm whose $q > 0.05$ (one-way ANOVA followed by a local FDR correction) were automatically moved to distribution 2. Because six hypothalamic metabolites could not be measured at 30°C, they were not classified into any group.

Metabolite clustering was performed with the function *hclust* from the R package stats, grouping objects based on Pearson correlation distance. Outliers were not removed.

Network analysis was performed with the R package *igraph* by considering only pairs of metabolites with a Pearson correlation coefficient above 0.6. Outliers were not removed. Ten mice were used for each group, except for AL at 22°C (nine mice). All 90 plasma metabolites and 37 hypothalamic metabolites were used to compute the correlations [all metabolites found except those hypothalamic metabolites that were measured at 22°C but could not be found at 30°C: PC(32:0), SM(d18:1/17:0), erythro-sphingosine, arachidonoylglycerol, $NADP^+$, and homoarginine]. The number of samples used to calculate the correlation between any two metabolites was the same (39 samples at 22°C and 40 samples at 30°C).

Chord diagrams were depicted with the R package *circlize* by considering only pairs of metabolites with a Pearson correlation coefficient above 0.6. The arc of circumference is proportional to the total number of correlations of each group and subgroup. For the sake of simplicity in the visualization of correlations, ribbons are duplicated. For example, ribbon size showing the number of correlations between lipids and amino acids is shown in red starting in the lipid sector and in blue (with the same size) starting from the amino acid sector. Outliers were not removed.

The intensity and diameter of the circumferences correspond to the mean Pearson correlation coefficient between two metabolites that appear in plasma and the hypothalamus. Outliers were not removed. Pathway enrichment was performed by using the WikiPathways database and a custom script using each metabolite's fold change.

Statistics

For untargeted metabolomics experiments, 10 mice per time point were used, except for the AL group at 22°C, which contained 9 animals. Data were presented as box-and-whisker plots showing the data from all mice analyzed. Outliers were not removed. Multigroup statistical significance of each feature was automatically determined by XCMS Online (*67*) using a one-way ANOVA followed by a local FDR correction of the *P* values to generate the corresponding *q* values. Features were considered as statistically significantly altered when the FDR was $q < 0.05$. Once metabolites were identified, for the pairwise comparison of each CR time point with AL feeding, a Tukey's honestly significant difference (HSD) post hoc test (parametric) was carried out. Metabolites were considered as statistically significantly altered at either CR time point (O, M, or T) with respect to AL feeding when $P < 0.05$.

For physiological parameters, repeated measures two-way ANOVA followed by Bonferroni's multiple comparison correction was used to analyze differences between treatments and T_a groups on T_b, locomotor activity, energy expenditure, and RER. GraphPad Prism 7 was used for data analysis of physiological parameters.

SUPPLEMENTARY MATERIALS

stke.sciencemag.org/cgi/content/full/13/648/eabb2490/DC1

Fig. S1. Body weight, body composition, and temperature at each tissue collection time point.
Fig. S2. Classification of metabolites based on the impact of diet or/and temperature.
Fig. S3. Effect of thermoneutrality on intertissue correlations.
Fig. S4. Temperature dictates fuel use and energy expenditure during CR.
Fig. S5. Cognitive prioritization of metabolites.
Fig. S6. The citrulline-NO cycle and polyamine metabolism are affected by housing temperature.
Data file S1. Plasma metabolite area and SD at both temperatures with statistics.
Data file S2. Hypothalamus metabolite area and SD at both temperatures with statistics.
Data file S3. Pathway enrichment analysis for plasma and hypothalamus metabolites.
Data file S4. Intra- and intertissue correlations.
Data file S5. Glucogenic amino acids in plasma.
Data file S6. Cognitive prioritization of metabolites.
Data file S7. Core body temperature of mice during CR with statistics.
Data file S8. Locomotor activity of mice during CR with statistics.
Data file S9. RER of mice during CR with statistics.
Data file S10. Energy expenditure of mice during CR with statistics.
Data file S11. Body weight of mice during CR with statistics.

View/request a protocol for this paper from *Bio-protocol*.

REFERENCES AND NOTES

1. W. Mair, A. Dillin, Aging and survival: The genetics of life span extension by dietary restriction. *Annu. Rev. Biochem.* **77**, 727–754 (2008).
2. C. H. O'Flanagan, L. A. Smith, S. B. McDonell, S. D. Hursting, When less may be more: Calorie restriction and response to cancer therapy. *BMC Med.* **15**, 106 (2017).
3. M. M. Y. Sung, J. R. B. Dyck, Age-related cardiovascular disease and the beneficial effects of calorie restriction. *Heart Fail. Rev.* **17**, 707–719 (2012).
4. M. J. Schafer, M. J. Alldred, S. H. Lee, M. E. Calhoun, E. Petkova, P. M. Mathews, S. D. Ginsberg, Reduction of β-amyloid and γ-secretase by calorie restriction in female Tg2576 mice. *Neurobiol. Aging* **36**, 1293–1302 (2015).
5. G. Testa, F. Biasi, G. Poli, E. Chiarpotto, Calorie restriction and dietary restriction mimetics: A strategy for improving healthy aging and longevity. *Curr. Pharm. Des.* **20**, 2950–2977 (2014).
6. M. A. Lane, D. J. Baer, W. V. Rumpler, R. Weindruch, D. K. Ingram, E. M. Tilmont, R. G. Cutler, G. S. Roth, Calorie restriction lowers body temperature in rhesus monkeys, consistent with a postulated anti-aging mechanism in rodents. *Proc. Natl. Acad. Sci. U.S.A.* **93**, 4159–4164 (1996).
7. A. Soare, R. Cangemi, D. Omodei, J. O. Holloszy, L. Fontana, Long-term calorie restriction, but not endurance exercise, lowers core body temperature in humans. *Aging* **3**, 374–379 (2011).
8. G. S. Roth, M. A. Lane, D. K. Ingram, J. A. Mattison, D. Elahi, J. D. Tobin, D. Muller, E. J. Metter, Biomarkers of caloric restriction may predict longevity in humans. *Science* **297**, 811 (2002).
9. J. R. Speakman, S. E. Mitchell, Caloric restriction. *Mol. Aspects Med.* **32**, 159–221 (2011).
10. R. Cintron-Colon, M. Sanchez-Alavez, W. Nguyen, S. Mori, R. Gonzalez-Rivera, T. Lien, T. Bartfai, S. Aid, J.-C. François, M. Holzenberger, B. Conti, Insulin-like growth factor 1 receptor regulates hypothermia during calorie restriction. *Proc. Natl. Acad. Sci. U.S.A.* **114**, 9731–9736 (2017).
11. G. Abreu-Vieira, C. Xiao, O. Gavrilova, M. L. Reitman, Integration of body temperature into the analysis of energy expenditure in the mouse. *Mol. Metab.* **4**, 461–470 (2015).
12. S. J. Swoap, M. J. Gutilla, Cardiovascular changes during daily torpor in the laboratory mouse. *Am. J. Physiol. Regul. Integr. Comp. Physiol.* **297**, R769–R774 (2009).
13. B. Conti, M. Sanchez-Alavez, R. Winsky-Sommerer, M. C. Morale, J. Lucero, S. Brownell, V. Fabre, S. Huitron-Resendiz, S. Henriksen, E. P. Zorrilla, L. de Lecea, T. Bartfai, Transgenic mice with a reduced core body temperature have an increased life span. *Science* **314**, 825–828 (2006).
14. J. Waalen, J. N. Buxbaum, Is older colder or colder older? The association of age with body temperature in 18,630 individuals. *J. Gerontol. A Biol. Sci. Med. Sci.* **66**, 487–492 (2011).
15. M. Protsiv, C. Ley, J. Lankester, T. Hastie, J. Parsonnet, Decreasing human body temperature in the United States since the industrial revolution. *eLife* **9**, e49555 (2020).
16. B. Conti, M. Hansen, A cool way to live long. *Cell* **152**, 671–672 (2013).
17. S.-J. Lee, C. Kenyon, Regulation of the longevity response to temperature by thermosensory neurons in *Caenorhabditis elegans*. *Curr. Biol.* **19**, 715–722 (2009).
18. G. B. Carvalho, I. Drago, S. Hoxha, R. Yamada, O. Mahneva, K. D. Bruce, A. Soto Obando, B. Conti, W. W. Ja, The 4E-BP growth pathway regulates the effect of ambient temperature on Drosophila metabolism and lifespan. *Proc. Natl. Acad. Sci. U.S.A.* **114**, 9737–9742 (2017).
19. R. Xiao, B. Zhang, Y. Dong, J. Gong, T. Xu, J. Liu, X. Z. S. Xu, A genetic program promotes *C. elegans* longevity at cold temperatures via a thermosensitive TRP channel. *Cell* **152**, 806–817 (2013).
20. I. Dickson, NAFLD: Thermoneutral housing of mice improves modelling of NAFLD. *Nat. Rev. Gastroenterol. Hepatol.* **14**, 451 (2017).

Downloaded from http://stke.sciencemag.org/ on October 29, 2020

21. D. A. Giles, M. E. Moreno-Fernandez, T. E. Stankiewicz, S. Graspeuntner, M. Cappelletti, D. Wu, R. Mukherjee, C. C. Chan, M. J. Lawson, J. Klarquist, A. Sünderhauf, S. Softic, C. R. Kahn, K. Stemmer, Y. Iwakura, B. J. Aronow, R. Karns, K. A. Steinbrecher, C. L. Karp, R. Sheridan, S. K. Shanmukhappa, D. Reynaud, D. B. Haslam, C. Sina, J. Rupp, S. P. Hogan, S. Divanovic, Thermoneutral housing exacerbates nonalcoholic fatty liver disease in mice and allows for sex-independent disease modeling. *Nat. Med.* **23**, 829–838 (2017).
22. X. Y. Tian, K. Ganeshan, C. Hong, K. D. Nguyen, Y. Qiu, J. Kim, R. K. Tangirala, P. Tontonoz, A. Chawla, Thermoneutral housing accelerates metabolic inflammation to potentiate atherosclerosis but not insulin resistance. *Cell Metab.* **23**, 165–178 (2016).
23. A. Koizumi, Y. Wada, M. Tuskada, T. Kayo, M. Naruse, K. Horiuchi, T. Mogi, M. Yoshioka, M. Sasaki, Y. Miyamaura, T. Abe, K. Ohtomo, R. L. Walford, A tumor preventive effect of dietary restriction is antagonized by a high housing temperature through deprivation of torpor. *Mech. Ageing Dev.* **92**, 67–82 (1996).
24. C. Guijas, J. R. Montenegro-Burke, B. Warth, M. E. Spilker, G. Siuzdak, Metabolomics activity screening for identifying metabolites that modulate phenotype. *Nat. Biotechnol.* **36**, 316–320 (2018).
25. M. M. Rinschen, J. Ivanisevic, M. Giera, G. Siuzdak, Identification of bioactive metabolites using activity metabolomics. *Nat. Rev. Mol. Cell Biol.* **20**, 353–367 (2019).
26. B. Warth, S. Spangler, M. Fang, C. H. Johnson, E. M. Forsberg, A. Granados, R. L. Martin, X. Domingo-Almenara, T. Huan, D. Rinehart, J. R. Montenegro-Burke, B. Hilmers, A. Aisporna, L. T. Hoang, W. Uritboonthai, H. P. Benton, S. D. Richardson, A. J. Williams, G. Siuzdak, Exposome-scale investigations guided by global metabolomics, pathway analysis, and cognitive computing. *Anal. Chem.* **89**, 11505–11513 (2017).
27. Y. Chen, E. Argentinis, G. Weber, IBM Watson: How cognitive computing can be applied to big data challenges in life sciences research. *Clin. Ther.* **38**, 688–701 (2016).
28. X. Domingo-Almenara, J. R. Montenegro-Burke, C. Guijas, E. L.-W. Majumder, H. P. Benton, G. Siuzdak, Autonomous METLIN-guided in-source fragment annotation for untargeted metabolomics. *Anal. Chem.* **91**, 3246–3253 (2019).
29. X. Domingo-Almenara, J. R. Montenegro-Burke, H. P. Benton, G. Siuzdak, Annotation: A computational solution for streamlining metabolomics analysis. *Anal. Chem.* **90**, 480–489 (2017).
30. A. Gomez-Muñoz, N. Presa, A. Gomez-Larrauri, I.-G. Rivera, M. Trueba, M. Ordoñez, Control of inflammatory responses by ceramide, sphingosine 1-phosphate and ceramide 1-phosphate. *Prog. Lipid Res.* **61**, 51–62 (2016).
31. T.-H. Collet, T. Sonoyama, E. Henning, J. M. Keogh, B. Ingram, S. Kelway, L. Guo, I. S. Farooqi, A metabolomic signature of acute caloric restriction. *J. Clin. Endocrinol. Metab.* **102**, 4486–4495 (2017).
32. S. J. Mitchell, J. Madrigal-Matute, M. Scheibye-Knudsen, E. Fang, M. Aon, J. A. González-Reyes, S. Cortassa, S. Kaushik, M. Gonzalez-Freire, B. Patel, D. Wahl, A. Ali, M. Calvo-Rubio, M. I. Buron, V. Guiterrez, T. M. Ward, H. H. Palacios, H. Cai, D. W. Frederick, C. Hine, F. Broeskamp, L. Habering, J. Dawson, T. M. Beasley, J. Wan, Y. Ikeno, G. Hubbard, K. G. Becker, Y. Zhang, V. A. Bohr, D. L. Longo, P. Navas, L. Ferrucci, D. A. Sinclair, P. Cohen, J. M. Egan, J. R. Mitchell, J. A. Baur, D. B. Allison, R. M. Anson, J. M. Villalba, F. Madeo, A. M. Cuervo, K. J. Pearson, D. K. Ingram, M. Bernier, R. de Cabo, Effects of sex, strain, and energy intake on hallmarks of aging in mice. *Cell Metab.* **23**, 1093–1112 (2016).
33. J. Yip, X. Geng, J. Shen, Y. Ding, Cerebral gluconeogenesis and diseases. *Front. Pharmacol.* **7**, 521 (2016).
34. S. R. Spindler, J. M. Dhahbi, P. L. Mote, in *Advances in Cell Aging and Gerontology*, M. P. Mattson, Ed. (Elsevier, 2003), vol. 14, pp. 69–86.
35. S. B. Heymsfield, C. Arteaga, C. McManus, J. Smith, S. Moffitt, Measurement of muscle mass in humans: Validity of the 24-hour urinary creatinine method. *Am. J. Clin. Nutr.* **37**, 478–494 (1983).
36. R. F. Vesali, M. Klaude, L. Thunblad, O. E. Rooyackers, J. Wernerman, Contractile protein breakdown in human leg skeletal muscle as estimated by [$^2H_3$]-3-methylhistidine: A new method. *Metabolism* **53**, 1076–1080 (2004).
37. C. Ardianto, N. Yonemochi, S. Yamamoto, L. Yang, F. Takenoya, S. Shioda, H. Nagase, H. Ikeda, J. Kamei, Opioid systems in the lateral hypothalamus regulate feeding behavior through orexin and GABA neurons. *Neuroscience* **320**, 183–193 (2016).
38. T. A. Czyzyk, R. Nogueiras, J. F. Lockwood, J. H. McKinzie, T. Coskun, J. E. Pintar, C. Hammond, M. H. Tschöp, M. A. Statnick, κ-Opioid receptors control the metabolic response to a high-energy diet in mice. *FASEB J.* **24**, 1151–1159 (2010).
39. F. S. Tepperman, M. Hirst, Effect of intrahypothalamic injection of [D-Ala^2,D-Leu^5] enkephalin on feeding and temperature in the rat. *Eur. J. Pharmacol.* **96**, 243–249 (1983).
40. R. Cintron-Colon, C. W. Johnson, J. R. Montenegro-Burke, C. Guijas, L. Faulhaber, M. Sanchez-Alavez, C. A. Aguirre, K. Shankar, M. Singh, A. Galmozzi, G. Siuzdak, E. Saez, B. Conti, Activation of kappa opioid receptor regulates the hypothermic response to calorie restriction and limits body weight loss. *Curr. Biol.* **29**, 4291–4299.e4 (2019).
41. S. M. Morris Jr., Arginine metabolism revisited. *J. Nutr.* **146**, 2579S–2586S (2016).
42. A. Haghikia, A. A. Kayacelebi, B. Beckmann, E. Hanff, R. Gold, A. Haghikia, D. Tsikas, Serum and cerebrospinal fluid concentrations of homoarginine, arginine, asymmetric and symmetric dimethylarginine, nitrite and nitrate in patients with multiple sclerosis and neuromyelitis optica. *Amino Acids* **47**, 1837–1845 (2015).
43. U. Forstermann, W. C. Sessa, Nitric oxide synthases: Regulation and function. *Eur. Heart J.* **33**, 829–837 (2011).
44. K. Yamada, M. Hiramatsu, Y. Noda, T. Mamiya, M. Murai, T. Kameyama, Y. Komori, T. Nikai, H. Sugihara, T. Nabeshima, Role of nitric oxide and cyclic GMP in the dizocilpine-induced impairment of spontaneous alternation behavior in mice. *Neuroscience* **74**, 365–374 (1996).
45. T. Eisenberg, M. Abdellatif, S. Schroeder, U. Primessnig, S. Stekovic, T. Pendl, A. Harger, J. Schipke, A. Zimmermann, A. Schmidt, M. Tong, C. Ruckenstuhl, C. Dammbrueck, A. S. Gross, V. Herbst, C. Magnes, G. Trausinger, S. Narath, A. Meinitzer, Z. Hu, A. Kirsch, K. Eller, D. Carmona-Gutierrez, S. Büttner, F. Pietrocola, O. Knittelfelder, E. Schrepfer, P. Rockenfeller, C. Simonini, A. Rahn, M. Horsch, K. Moreth, J. Beckers, H. Fuchs, V. Gailus-Durner, F. Neff, D. Janik, B. Rathkolb, J. Rozman, M. H. de Angelis, T. Moustafa, G. Haemmerle, M. Mayr, P. Willeit, M. von Frieling-Salewsky, B. Pieske, L. Scorrano, T. Pieber, R. Pechlaner, J. Willeit, S. J. Sigrist, W. A. Linke, C. Mühlfeld, J. Sadoshima, J. Dengjel, S. Kiechl, G. Kroemer, S. Sedej, F. Madeo, Cardioprotection and lifespan extension by the natural polyamine spermidine. *Nat. Med.* **22**, 1428–1438 (2016).
46. M. Filfan, A. Olaru, I. Udristoiu, C. Margaritescu, E. Petcu, D. M. Hermann, A. Popa-Wagner, Long-term treatment with spermidine increases health span of middle-aged Sprague-Dawley male rats. *Geroscience* **42**, 937–949 (2020).
47. F. Madeo, D. Carmona-Gutierrez, O. Kepp, G. Kroemer, Spermidine delays aging in humans. *Aging* **10**, 2209–2211 (2018).
48. F. Madeo, T. Eisenberg, F. Pietrocola, G. Kroemer, Spermidine in health and disease. *Science* **359**, eaan2788 (2018).
49. K. Nishimura, R. Shiina, K. Kashiwagi, K. Igarashi, Decrease in polyamines with aging and their ingestion from food and drink. *J. Biochem.* **139**, 81–90 (2006).
50. R. Cintron-Colon, K. Shankar, M. Sanchez-Alavez, B. Conti, Gonadal hormones influence core body temperature during calorie restriction. *Temperature (Austin)* **6**, 158–168 (2019).
51. C. Chevalier, O. Stojanović, D. J. Colin, N. Suarez-Zamorano, V. Tarallo, C. Veyrat-Durebex, D. Rigo, S. Fabbiano, A. Stevanović, S. Hagemann, X. Montet, Y. Seimbille, N. Zamboni, S. Hapfelmeier, M. Trajkovski, Gut microbiota orchestrates energy homeostasis during cold. *Cell* **163**, 1360–1374 (2015).
52. S. Fabbiano, N. Suárez-Zamorano, C. Chevalier, V. Lazarević, S. Kieser, D. Rigo, S. Leo, C. Veyrat-Durebex, N. Gaïa, M. Maresca, D. Merkler, M. Gomez de Agüero, A. Macpherson, J. Schrenzel, M. Trajkovski, Functional gut microbiota remodeling contributes to the caloric restriction-induced metabolic improvements. *Cell Metab.* **28**, 907–921.e7 (2018).
53. S. Fujisaka, J. Avila-Pacheco, M. Soto, A. Kostic, J. M. Dreyfuss, H. Pan, S. Ussar, E. Altindis, N. Li, L. Bry, C. B. Clish, C. R. Kahn, Diet, genetics, and the gut microbiome drive dynamic changes in plasma metabolites. *Cell Rep.* **22**, 3072–3086 (2018).
54. M. Zimmermann, M. Zimmermann-Kogadeeva, R. Wegmann, A. L. Goodman, Mapping human microbiome drug metabolism by gut bacteria and their genes. *Nature* **570**, 462–467 (2019).
55. H. Togashi, I. Sakuma, M. Yoshioka, T. Kobayashi, H. Yasuda, A. Kitabatake, H. Saito, S. S. Gross, R. Levi, A central nervous system action of nitric oxide in blood pressure regulation. *J. Pharmacol. Exp. Ther.* **262**, 343–347 (1992).
56. S. Bröer, A. Bröer, Amino acid homeostasis and signalling in mammalian cells and organisms. *Biochem. J.* **474**, 1935–1963 (2017).
57. G. A. Soultoukis, L. Partridge, Dietary protein, metabolism, and aging. *Annu. Rev. Biochem.* **85**, 5–34 (2016).
58. S. M. Solon-Biet, A. C. McMahon, J. W. O. Ballard, K. Ruohonen, L. E. Wu, V. C. Cogger, A. Warren, X. Huang, N. Pichaud, R. G. Melvin, R. Gokarn, M. Khalil, N. Turner, G. J. Cooney, D. A. Sinclair, D. Raubenheimer, D. G. Le Couteur, S. J. Simpson, The ratio of macronutrients, not caloric intake, dictates cardiometabolic health, aging, and longevity in ad libitum-fed mice. *Cell Metab.* **19**, 418–430 (2014).
59. N. E. Cummings, E. M. Williams, I. Kasza, E. N. Konon, M. D. Schaid, B. A. Schmidt, C. Poudel, D. S. Sherman, D. Yu, S. I. Arriola Apelo, S. E. Cottrell, G. Geiger, M. E. Barnes, J. A. Wisinski, R. J. Fenske, K. A. Matkowskyj, M. E. Kimple, C. M. Alexander, M. J. Merrins, D. W. Lamming, Restoration of metabolic health by decreased consumption of branched-chain amino acids. *J. Physiol.* **596**, 623–645 (2018).
60. W.-C. Mu, E. VanHoosier, C. M. Elks, R. W. Grant, Long-term effects of dietary protein and branched-chain amino acids on metabolism and inflammation in mice. *Nutrients* **10**, 918 (2018).
61. F. Vanden Abeele, A. Zholos, G. Bidaux, Y. Shuba, S. Thebault, B. Beck, M. Flourakis, Y. Panchin, R. Skryma, N. Prevarskaya, Ca^{2+}-independent phospholipase A_2-dependent gating of TRPM8 by lysophospholipids. *J. Biol. Chem.* **281**, 40174–40182 (2006).
62. V. V. Feketa, S. P. Marrelli, Induction of therapeutic hypothermia by pharmacological modulation of temperature-sensitive TRP channels: Theoretical framework and practical considerations. *Temperature (Austin)* **2**, 244–257 (2015).
63. B.-K. Choi, T. Dayaram, N. Parikh, A. D. Wilkins, M. Nagarajan, I. B. Novikov, B. J. Bachman, S. Y. Jung, P. J. Haas, J. L. Labrie, C. R. Pickering, A. K. Adikesavan, S. Regenbogen, L. Kato, A. Lelescu, C. M. Buchovecky, H. Zhang, S. H. Bao, S. Boyer, G. Weber, K. L. Scott, Y. Chen, S. Spangler, L. A. Donehower, O. Lichtarge, Literature-based automated discovery of tumor suppressor p53 phosphorylation and inhibition by NEK2. *Proc. Natl. Acad. Sci. U.S.A.* **115**, 10666–10671 (2018).

Downloaded from http://stke.sciencemag.org/ on October 29, 2020

64. W. Francesconi, M. Sánchez-Alavez, F. Berton, S. Alboni, C. Benatti, S. Mori, W. Nguyen, E. Zorrilla, G. Moroncini, F. Tascedda, B. Conti, The proinflammatory cytokine interleukin 18 regulates feeding by acting on the bed nucleus of the stria terminalis. *J. Neurosci.* **36**, 5170–5180 (2016).
65. J. Ivanisevic, Z.-J. Zhu, L. Plate, R. Tautenhahn, S. Chen, P. J. O'Brien, C. H. Johnson, M. A. Marletta, G. J. Patti, G. Siuzdak, Toward 'omic scale metabolite profiling: A dual separation-mass spectrometry approach for coverage of lipid and central carbon metabolism. *Anal. Chem.* **85**, 6876–6884 (2013).
66. D. Kessner, M. Chambers, R. Burke, D. Agus, P. Mallick, ProteoWizard: Open source software for rapid proteomics tools development. *Bioinformatics* **24**, 2534–2536 (2008).
67. R. Tautenhahn, G. J. Patti, D. Rinehart, G. Siuzdak, XCMS Online: A web-based platform to process untargeted metabolomic data. *Anal. Chem.* **84**, 5035–5039 (2012).
68. C. Guijas, J. R. Montenegro-Burke, X. Domingo-Almenara, A. Palermo, B. Warth, G. Hermann, G. Koellensperger, T. Huan, W. Uritboonthai, A. E. Aisporna, D. W. Wolan, M. E. Spilker, H. P. Benton, G. Siuzdak, METLIN: A technology platform for identifying knowns and unknowns. *Anal. Chem.* **90**, 3156–3164 (2018).
69. X. Domingo-Almenara, J. R. Montenegro-Burke, J. Ivanisevic, A. Thomas, J. Sidibé, T. Teav, C. Guijas, A. E. Aisporna, D. Rinehart, L. Hoang, A. Nordström, M. Gómez-Romero, L. Whiley, M. R. Lewis, J. K. Nicholson, H. P. Benton, G. Siuzdak, XCMS-MRM and METLIN-MRM: A cloud library and public resource for targeted analysis of small molecules. *Nat. Methods* **15**, 681–684 (2018).

Funding: This research was partially funded by National Institutes of Health grants R35 GM130385, R01 GM114368, P30 MH062261, P01 DA026146, U01 CA235493 and the NIH Cloud Credits Model Pilot, a component of the NIH Big Data to Knowledge (BD2K) program (G.S.). This work has also been supported by the National Institutes of Health, GM113894 (B.C.). R.C.-C. was supported by the Skaggs Graduate School of Chemical and Biological Sciences and ARCS Foundation. **Author contributions:** C.G., J.R.M.-B., R.C.-C., G.S., and B.C. conceptualized and designed the methodology. C.G., J.R.M.-B., R.C.-C., X.D.-A., and E.B. designed software and performed formal analysis and data curation. C.G., J.R.M.-B., R.C.-C., M.S.-A., C.A.A., K.S., and E.L.-W.M. performed the investigation. J.R.M.-B. carried out chemical synthesis. C.G., R.C.-C., and B.C. wrote, reviewed, and edited the manuscript, with contributions of all other authors. G.S. and B.C. supervised and acquired funding. **Competing interests:** The authors declare that they have no competing interests. **Data and materials availability:** Raw data were deposited into the XCMS Online Public Repository (https://xcmsonline.scripps.edu/landing_page.php?pgcontent=listPublicShares) under the following job numbers: RP_Plasma_22C (1195307), HILIC_Plasma_22C (1199892), RP_Plasma_30C (1245492), HILIC_Plasma_30C (1246156), RP_Hypothalamus_22C (1200673), HILIC_Hypothalamus_22C (1200876), RP_Hypothalamus_30C (1250736), and HILIC_Hypothalamus_30C (1250484). All other data needed to evaluate the conclusions in the paper are present in the paper or the Supplementary Materials.

Submitted 11 February 2020
Accepted 7 August 2020
Published 8 September 2020
10.1126/scisignal.abb2490

Citation: C. Guijas, J. R. Montenegro-Burke, R. Cintron-Colon, X. Domingo-Almenara, M. Sanchez-Alavez, C. A. Aguirre, K. Shankar, E. L.-W. Majumder, E. Billings, B. Conti, G. Siuzdak, Metabolic adaptation to calorie restriction. *Sci. Signal.* **13**, eabb2490 (2020).

Downloaded from http://stke.sciencemag.org/ on October 29, 2020

Science Signaling

Metabolic adaptation to calorie restriction

Carlos Guijas, J. Rafael Montenegro-Burke, Rigo Cintron-Colon, Xavier Domingo-Almenara, Manuel Sanchez-Alavez, Carlos A. Aguirre, Kokila Shankar, Erica L.-W. Majumder, Elizabeth Billings, Bruno Conti and Gary Siuzdak

Sci. Signal. **13** (648), eabb2490.
DOI: 10.1126/scisignal.abb2490

Rewired into hypothermia by deprivation

Calorie restriction extends health span, which is thought to be mediated in part through a decrease in core body temperature. Guijas *et al.* compared metabolomics data from mice subjected to calorie restriction and that were housed at a temperature lower than body temperature or at thermoneutrality, reasoning that thermoneutrality would offset the metabolic changes induced by calorie restriction. The authors found that calorie restriction induced the hypothalamus to produce the gasotransmitter nitric oxide and the opioid peptide leucine enkephalin in mice housed at cooler temperature, but not in mice housed at thermoneutrality. These and other metabolites that were differentially altered by ambient temperature may form the basis for developing compounds that can deliver the beneficial effects of calorie restriction.

ARTICLE TOOLS http://stke.sciencemag.org/content/13/648/eabb2490

SUPPLEMENTARY MATERIALS http://stke.sciencemag.org/content/suppl/2020/09/03/13.648.eabb2490.DC1

RELATED CONTENT
http://stke.sciencemag.org/content/sigtrans/13/624/eaaz1482.full
http://stke.sciencemag.org/content/sigtrans/12/611/eaax9760.full
http://science.sciencemag.org/content/sci/362/6416/770.full
http://science.sciencemag.org/content/sci/359/6374/eaan2788.full
http://science.sciencemag.org/content/sci/314/5800/825.full
http://stm.sciencemag.org/content/scitransmed/12/555/eabd4765.full
http://advances.sciencemag.org/content/advances/6/1/eaaz1441.full
http://advances.sciencemag.org/content/advances/6/32/eaba1306.full
file:/content

REFERENCES This article cites 68 articles, 13 of which you can access for free
http://stke.sciencemag.org/content/13/648/eabb2490#BIBL

PERMISSIONS http://www.sciencemag.org/help/reprints-and-permissions

Use of this article is subject to the Terms of Service

Science Signaling (ISSN 1937-9145) is published by the American Association for the Advancement of Science, 1200 New York Avenue NW, Washington, DC 20005. The title *Science Signaling* is a registered trademark of AAAS.

Copyright © 2020 The Authors, some rights reserved; exclusive licensee American Association for the Advancement of Science. No claim to original U.S. Government Works

Downloaded from http://stke.sciencemag.org/ on October 29, 2020